Evolution of an oceanic anticyclone in the lee of Madeira Island: In situ and remote sensing survey

Rui M. A. Caldeira[1,2], Alexandre Stegner[3,4], Xavier Couvelard[2,5], Isabel B. Araújo[1], Pierre Testor[6], and Alvaro Lorenzo[7]

[1]CIIMAR-Interdisciplinary Centre of Marine and Environmental Research, University of Porto, Porto, Portugal, [2]CCM-Center for Mathematical Sciences, University of Madeira, Funchal, Portugal, [3]Laboratoire de Météorologie Dynamique, École Polytechnique, Palaiseau, Paris, France, [4]UME, ENSTA Centre de l'Yvette, Chemin de la Huniere, Palaiseau, Paris, France, [5]Laboratoire de Physique des Océans, Plouzané, France, [6]LOCEAN-IPSL, Laboratoire d'Oceanographie et du Climat, Université Pierre and Marie Curie, Paris, France, [7]PLOCAN-Plataforma Oceánica de Canarias, Las Palmas, Canary Islands, Spain

Abstract Island wakes are areas of a strong eddy activity influencing the availability and transport of organic matter in the ocean which, in turn impact biological productivity. Despite this, eddy formation in the lee of North Atlantic tropical islands is scarcely documented, except for the Canary Islands. Moreover, the occurrence of anticyclones leeward of Madeira has seldom been detected. During the summer of 2011, a multiplatform approach, combining satellite data with in situ measurements, was used to study an anticyclonic eddy generated in the lee of the Madeira Island. The main objective was to confirm recent numerical evidence suggesting that orographically perturbed winds can induce anticyclonic eddies leeward of Madeira, particularly during summer months. The high resolution sampling of the eddy's interior shows a strong downwelling of $\approx$100 m of the isopycnal layer below the mixed layer, typical of intrathermocline eddies. The 25 km radius of this anticyclonic structure exceeds the local deformation radius by a factor of 2. The vortex Rossby number remained moderate (Ro = 0.26) even if the relative core vorticity reached a finite value ($\zeta/f = -0.7$). The occurrence of strong trade winds (10–15 m s^{-1}) prior to the detection of the first surface eddy signatures (July 2011) concurrent with opposite flowing geostrophic currents, shows that the orographic wind forcing is the main mechanism for generating this mesoscale long-lived eddy. After leaving the shelter of the island, the eddy traveled northwesterly following a perpendicular net Ekman transport pathway at a speed of 5 km/d, for at least 2 months. An interaction with a cyclonic partner generated in the area helped precipitate the northward trajectory. This study presents the first clear evidence of a wind-induced mesoscale anticyclone in the lee of Madeira.

1. Introduction

Island wakes are the location of a strong eddy activity, which have important biological consequences to the formation and transport of organic matter. Cyclonic vortices bring nutrients from deeper-layers into the euphotic zone, promoting biological growth [*Hasegawa*, 2004; *Hasegawa et al.*, 2009], whereas anticyclones are known to concentrate and transport biological matter in the upper thermocline over long distances [*Mackas and Galbraith*, 2002; *Ladd et al.*, 2009; *Jia et al.*, 2011]. Thus, cyclonic eddies have a cold core of upwelled water at the surface while anticyclonic vortices are characterized by a warm surface signature [*Arístegui et al.*, 1994; *Caldeira et al.*, 2002; *Caldeira and Marchesiello*, 2002]. Both cyclonic and anticyclonic eddies can be detected by altimetry data. However, due to its coarser resolution (1/3°) the vortex detection from sea surface height anomalies are restricted to large mesoscale eddies. Higher resolution is available on thermal sensors (up to 250 m for MODIS) but due to intense solar radiation and clear skies a warm wake is omnipresent during the summer months leeward of subtropical islands such as Madeira and Canaries. This phenomena could mask the high Sea Surface Temperature (SST) signature characteristic of anticyclonic eddies [*Caldeira et al.*, 2002]. Hence, the remote sensing detection of warm anticyclones in the near wake is probably less efficient than in the open ocean. Therefore, in order to fully characterize island wake eddies it is necessary to perform a multiplatform survey, combining satellite products with in situ measurements supplemented by numerical and laboratory studies.

Several studies have sampled cyclones and anticyclones forming leeward of islands and archipelagos located in the deep ocean [*Sangrà*, 2005; *Sangrà et al.*, 2007; *Hasegawa*, 2004; *Chavanne et al.*, 2010; *Jia et al.*, 2011].

However, the various oceanic or atmospheric mechanisms which favor the formation of these coherent oceanic features in the wake of islands are still under discussion. For flat islands, there is no significant wind curl forcing the ocean, eddies are mainly generated by the lateral friction induced by the interaction between the island bathymetry and the oceanic incoming flow. In the framework of nonrotating and barotropic flows, the dynamical properties of the vortex street is controlled by the Reynolds number ($Re=UD/\nu$) and a periodic shedding occurs when it exceeds the critical value $Re=UD/\nu > 45-50$ [*Jackson*, 2006; *Wen and Lin*, 2001]. However, there are some practical challenges in estimating the effective Reynolds number around islands because the lateral dissipation is highly turbulent and nonuniform. In oceanic conditions, the molecular viscosity (ν) is replaced by an equivalent horizontal eddy viscosity (a.k.a. Austausch coefficient) [*Tomczak*, 1988]. Hence, the critical threshold for vortex shedding is hard to estimate with accuracy. Nevertheless, if the upstream current is strong enough and impacts the island, a periodic eddy shedding is expected to occur, as it is the case for the classical two-dimensional Von Karman Vortex Street. In such circumstances, the size of the wake vortices are comparable to the effective island radius R and the eddy intensity is mainly controlled by the incoming current velocity U (the island diameter $D = 2R$). Hence, a moderate geostrophic flow interacting with a deep oceanic island will lead to the generation of leeward geostrophic eddies of both signs [*Dietrich et al.*, 1996; *Heywood et al.*, 1996; *Coutis and Middleton*, 2002]. On the other hand, strong currents such as the Kuroshio impinging on a small island ($D = 5 - 10$ km), such as the Aoga-Shima Island [*Hasegawa et al.*, 2009] or the Green Island [*Chang et al.*, 2013] may lead to the formation of intense submesoscale cyclones only. Indeed, when the relative vorticity (ζ/f) becomes finite, inertial instability may strongly destabilize and disintegrate the anticyclones [*Stegner et al.*, 2005; *Dong and McWilliams*, 2007; *Hasegawa et al.*, 2009; *Teinturier et al.*, 2010; *Lazar et al.*, 2013a]. In such cases, unlike the standard Von Karman Vortex street the leeward eddies are mainly cyclonic. Contrary to what was originally thought in the scientific literature, to take into account this ageostrophic instability, the earth rotation should be taken into account even for small-scale islands, i.e., $D << R_d$. Hence, we often use the island Rossby number ($Ro=U/fR$) to estimate the relative intensity of wake vortices. Recent studies have shown that we should also take into account the relative size of the island (or the eddies) in comparison with the first baroclinic deformation radius (R_d) calculated from the local stratification. In the oceans, R_d could be comparable or smaller than typical islands radius R and the dimensionless Burger number ($Bu=(R_d/R)^2$), which quantifies the ratio of the kinetic to the potential energy, must also be considered. Idealized laboratory experiments [*Perret et al.*, 2006a, 2006b] and numerical simulations [*Perret et al.*, 2006a, 2006b; *Dong et al.*, 2007], have shown that when the ratio Ro/Bu becomes large, anticyclones remain coherent and circular, whereas cyclones tend to be elongated and distorted. For some extreme cases, coherent cyclones do not emerge at all, and only anticyclonic vortices appear several diameters behind a circular island [*Perret et al.*, 2006a, 2006b]. Hence, dynamically the cyclone-anticyclone asymmetry of the wake pattern, in the lee of deep oceanic islands, is controlled by at least two main parameters: Ro and Bu, respectively [*Stegner*, 2014].

For oceanic mountainous islands, the role of the local wind stress as a driver of oceanic vortices was first noted by *Patzert* [1969], in a discussion of the role of Ekman pumping in generating Hawaiian lee eddies. This was highlighted in recent numerical studies [*Calil et al.*, 2008; *Yoshida et al.*, 2010; *Jia et al.*, 2011; *Kersalé et al.*, 2011; *Couvelard et al.*, 2012]. For the Hawaiian case, the interaction between the North Equatorial Current and the archipelago is enough to generate eddies, but high resolution wind stress curl is needed to calculate the correct intensities of the vortices as observed from the altimetry [*Calil et al.*, 2008]. The role of wind forcing has also been discussed for the Canary Islands [*Barton et al.*, 2000; *Jiménez et al.*, 2008; *Piedeleu et al.*, 2009].

Madeira Island, located in the NE deep Atlantic Ocean has been the focus of some previous oceanographic studies [*Caldeira et al.*, 2002; *Caldeira and Sangrà*, 2012]. Cyclonic mesoscale eddies were predominant in simulated and/or remote sensing data of previous wake studies. Most recently, *Couvelard et al.* [2012] used a high resolution meteorological model to force an oceanic model representing the Madeira Archipelago. With the inclusion of Madeira orography in the perturbation of the incoming trade winds, the authors were able to replicate closer to realistic atmospheric and oceanic conditions, such that several cyclonic and anticyclonic oceanic eddies were generated leeward of the islands. The simulated anticyclones formed leeward of "Caniçal" (NE tip of Madeira Island), grew to dimensions comparable to the local deformation radius R_d before shedding southward, in a region confined to the island wake.

The current research uses several oceanic in situ measurements and remote sensing analysis, collected over a 6 month period (August 2011 to January 2012) in the lee of Madeira island, in order to study the evolution

of a mesoscale anticyclone first detected on the 21 August 2011. The sampling campaign was carried out in the scope of the ICOVBIO project, jointly organized by the Interdisciplinary Centre of Marine and Environmental Research (CIIMAR) and the "Laboratoire de Meteorologie Dynamique'e (CNRS)," with the participation of the Madeira Whale Museum. Therefore, the main objective of this study was to confirm recent numerical evidences which suggest that orographically perturbed winds could induce anticyclonic eddies leeward of Madeira, particularly during summer months [*Couvelard et al.*, 2012].

A description of the various instruments used during the campaign and the corresponding data processing procedures are detailed in section 2. The eddy dynamical properties and its relationship with the surroundings are presented in section 3. The conclusions are preceded by a discussion on the long-term evolution and on historical evidences of anticyclonic circulation occurring leeward of Madeira.

2. Instruments and Data Processing

A combination of ship-based Conductivity Temperature Depth (CTD), Autonomous Underwater Vehicle (AUV), and surface drifter measurements were collected in the scope of the ICOVBIO campaign from August 2011 to January 2012, in the lee of Madeira Archipelago. The Spanish PLOCAN team operated the AUVs in close cooperation with the French EGO team. The various instruments used during the campaign and the corresponding data processing procedures are detailed below.

2.1. Remote Sensing Data: MODIS and Altimetry

Surface chlorophyll (Chl-a), Sea Surface Temperature (SST), and Sea Surface Height (SSH) are satellite derived observations that can respond to eddy dynamics, i.e., proxies. For instance, satellite altimeters can detect anticyclonic eddies based on their negative sea level anomalies, which arise from surface convergence and downwelling.

The Moderate Resolution Imaging Spectroradiometer (MODIS) instrument flying aboard NASA Terra and Aqua satellites provides a daily (morning and afternoon) view of Madeira during the descending and ascending orbital passes, respectively. Its spatial resolution holds an advantage over Sea Surface Height (SSH) products. However, passive thermal and infrared sensors such as MODIS rely on cloud free vision of the ocean surface for measurements. For the near-real time support of the campaign, daily Level-2 (L2) standard chlorophyll and SST products were download from Ocean Color Web [*Feldman and McClain*, 2007] and mapped to a cylindrical coordinate system that retained the original 1 km spatial resolution. This level of processing was sufficient to locate an anticyclonic eddy forming south of Madeira Island and served to plan the ship-based hydrographic measurements. Post campaign, a selected number of images were chosen from all the available (2002–2012) L2 MODIS data [*Feldman and McClain*, 2012] that had been processed for a large domain around Madeira. These data were subsampled to 35° to 30°N and 19° to 15°W (the same region as the altimetry data) and processed to mapped level 3 (L3) (no spatial binning) images with high sun glint, high sensor view zenith angle and straylight contamination default flags. This allowed for a better representation of the spatial signature of the eddy.

Preprocessed Sea Level Anomaly (SLA) and absolute geostrophic velocity data were downloaded from AVISO website. Absolute geostrophic velocities were computed from absolute topography. The product is available at 1/3° × 1/3° spatial resolution, projected onto a Mercator-grid. AVISO gridded data sets for 2011 are based on two satellites (Jason-1/2 onboard of Envisat and Topex-Poseidon onboard of ERS) with concurrent ground tracks (http://www.aviso.oceanobs.com/duacs/).

2.2. CTD and UCTD Ship-Based Measurements

After detection, ship-based survey of the eddy was carried out using a combination of Conductivity Temperature Depth (CTD) sensor, and an Underway towed CTD system (UCTD). The CTD profiler was a SBE (Sea Bird Electronics) 19plus V2 SeaCAT Profiler, which sampled continuously at up to 4 scans per second (4 Hz) to a maximum depth of 600 m, with a vertical wire when the ship was in station. The UCTD manufactured by "Oceanscience" allowed to achieve over 500 m profiles, while the vessel was moving between stations at ∼ 8 kts, enabled the sampling of the eddy's interior at a much higher resolution. The UCTD was also fitted with a SBE sensor similar to the SBE-19 sampling at a much higher rate (16 Hz), achieving an overall depth resolution of about 25 cm, it attained a drop speed of about 4 ms^{-1}. A total of 30 good casts were completed in a 120 km transect during a period of 3 days, thus permitting a synoptic survey of the eddy before

it completed a full body rotation. A continuous record of time and position was maintain by the ship's electronic log, CTD casts and/or UCTD surface deployments were noted on the same log for future reference.

SBE software (Seasoft V2) was used to process all the CTD data. The processing was done in several steps: (i) the CTDs binary files were converted to engineering units; (ii) the data scans were aligned since the sensors are placed in slightly different physical positions on the CTD, thus measuring slightly different depth layers in profiling mode; (iii) sampling rates of the different sensors also had to be synchronized: (iv) Ship heave was removed, before (v) deriving the physical variables from the CTD original measures, including: salinity, density (sigma-t), potential temperature, and depth (using UNESCO equation of state). Only downcast data were extracted for further analysis in 2 m depth bins. The Ocean Data Viewer (ODV) was used to further analyze and represent the processed data including the calculation of Brunt-Väisälä frequencies and geostrophic currents.

2.3. MLI Drifters
Four MLI drifters with a "holey-sock" centered at 50 m were released near the eddy core, between the 26 and the 28 August 2011. Once activated, these buoys transmitted their hourly GPS positions via Iridium Satellite. A kringing method was used to filter the data and compute the drifter positions and speeds [*Poulain and Zambianchi*, 2007]. While they remained trapped, the drifters looped inside the anticyclone with a mean period of a few days. Hence, using a low-pass window, we filtered out these oscillations on both the latitude and the longitude axes, permitting the computation of the slow evolution of the eddy center. The mean trajectory of the core of the eddy was subsequently interpolated from the four drifters data set. The buoys positions were plotted either in the Earth frame using latitudes, longitudes coordinates, or in the moving frame of the eddy center using Cartesian coordinates (X,Y). Originally designed for the tuna fisheries, the MLI drifters are solar powered so that they can endure long deployment periods.

2.4. Autonomous Underwater Vehicle (AUV) Mission
A G2 Slocum Glider manufactured by Teledyne Webb research was launched from Madeira Island SE coast ("Caniçal") on the 11 September 2011. The mission lasted 20 days and during that period the AUV crossed the anticyclone twice. The G2 Slocum glider is unique in its class since it carries two computational units, one to process the navigational data and the other to process data obtained from the scientific sensors. This 2-unit configuration of the G2, enabled us to obtain high-frequency scientific data in conjunction with high-resolution navigational data. In its Madeira mission, the glider carried a pumped SBE 37 CTD with a FNLTU WetLab flurometer, which measured chlorophyll concentration and turbidity, all sampling at 3 Hz. In the deepest dives the AUV reached over 800 m, however, most of the sampling took place in the top 500 m of the water column.

In addition of being stored in memory cards on-board of the glider, part of the data was also transmitted via satellite link (hourly) to shore, enabling the scientific and piloting teams to make near real time decisions on where to send the AUV to. Daily adjustments were made depending on the drift of the glider and on the relative position of the eddy, according to information obtained from the satellite data and from the plots obtained with data from the glider on-board sensors (e.g., CTDs; navigation; etc.). After recovering the glider the full navigational and scientific data set was retrieved. Some preprocessing routines were used to filtered the large data set for further analysis, including: (i) removal of empty columns and NaN values and (ii) converting binary variables to valid engineering units. Processing of the on-board CTD data followed the same procedures as described above, averaged over 1 m depth bins.

3. Hydrographic and Dynamical Eddy Characterization

3.1. Surface Signatures
Sub and mesoscales eddies are often revealed at the surface by the advection of surfactants including chlorophyll-rich organisms. In fact, the high resolution MODIS ocean color data unveiled chlorophyll filaments swirling in an anticyclonic motion on the 21 August 2011, in the lee of Madeira island (Figure 1a). High chlorophyll concentration was also visible on the north-east side of Madeira Archipelago (Desertas Islands). The high contrast of this image played a crucial role in the location of the eddy center at the planning stages of the ICOVBIO campaign. A similar chlorophyll swirling pattern remained visible 2 weeks later, on the 6 October (Figure 1c). Both chlorophyll images also showed an interaction of the anticyclone with an
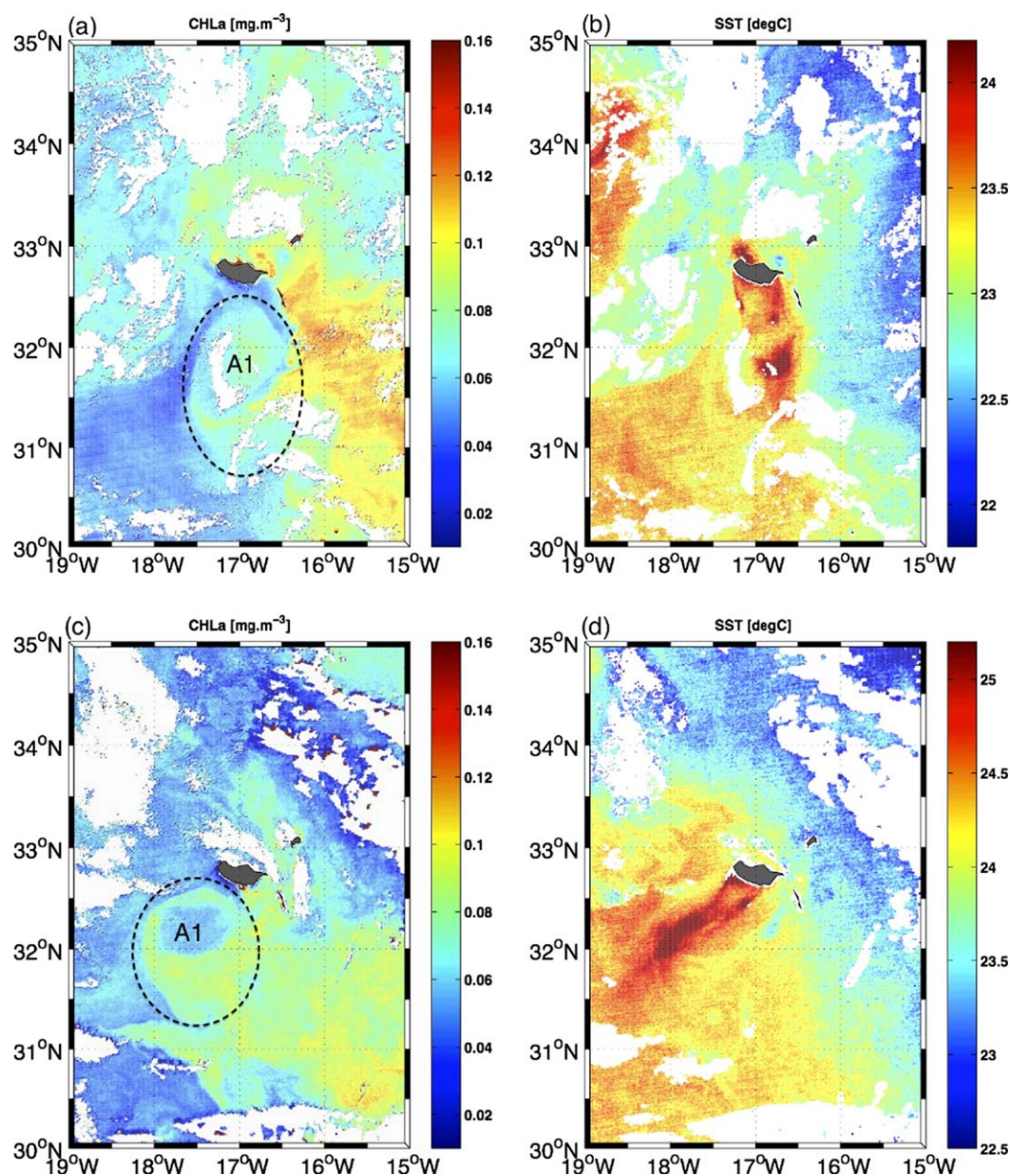
Figure 1. SST (°C) and sea surface chlorophyll (mg m^{-3}) signature of a mesoscale anticyclonic eddy in the south of Madeira island. (a) Chlorophyll-a concentration for the 21 August 2011; (b) SST for 21 August 2011; (c) Chl-a concentration for the 6 October 2011; and (d) SST for the 6 October 2011. Level-3 data from MODIS.

oligotrophic water filament (deep blue color, Figures 1a and 1c) on the south-west side of Madeira. An apparent evolution of the anticyclone is also visible. On the 21 August it had a productive (high chlorophyll concentration) core, whereas on the 6 October the core became oligotrophic, maintaining a productive rim. Some of the productive water inside the anticyclone seemed to have been advected for the north-east part of the Archipelago (Desertas Islands). In that case, the anticyclonic core corresponded to an unproductive feature, which entrained productive surface water from the nearby coastal regions. This supports the role of anticyclones as vehicles of transport of organic matter, previously discussed by several authors [*Mackas and Galbraith*, 2002; *Ladd*, 2005; *Jia et al.*, 2011]. Despite the extensive remote sensing database collected and analyzed, these MODIS images represent the best evidences of the near-field impact of the anticyclonic circulation on the surface chlorophyll during the ICOVBIO campaign. Sea surface temperatures provided further elements for the discussion.
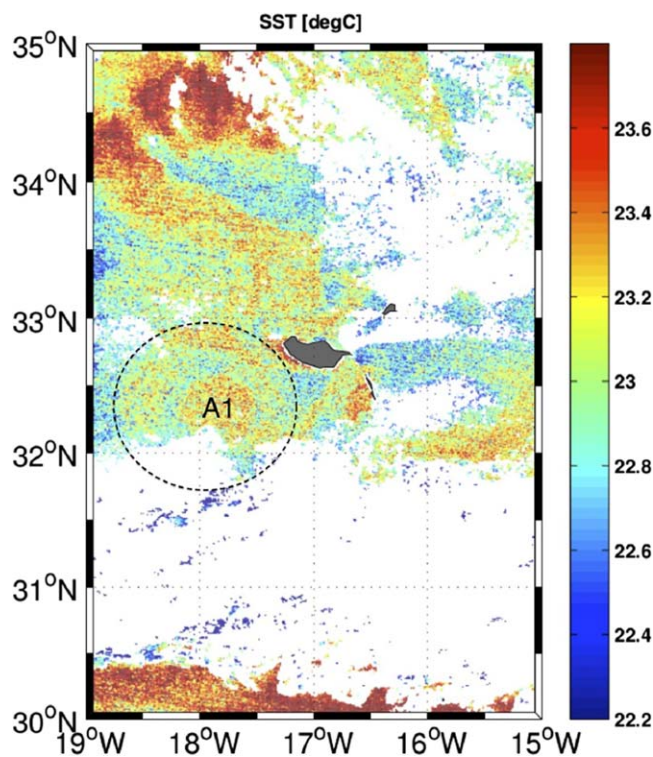
Figure 2. SST (°C) for 11 October 2011, showing the SST signature of the anticyclone formed leeward of Madeira Island. Level-3 data from MODIS.

A large-scale anticyclone should exhibit a core region of warm water, but in the lee of mountainous islands, intensively affected by the wind regimes, such signature could be masked by the occurrence of a warm wake formed by exposure of the sea surface to intense solar radiation. Daytime heating and the absence of strong winds in the lee will generally induce a thin warm stratified surface layer in the south of Madeira Island during summer months [*Caldeira et al.*, 2002; *Caldeira and Tomé*, 2013]. This warm wake was visible on the 21 August and on the 6 October images (Figures 1b and 1d), with a significant impact on the surface temperature. The warm core of the anticyclonic circulation was therefore masked by the warm wake. Without the occurrence of a warm wake, the SST for the 11 October does reveal the warm signature of the anticyclone (Figure 2). Considering that warm wakes frequently form in this region during summer months, it becomes hard to detect the presence of a large and coherent anticyclones solely from SST, other data sets less affected by clouds must be considered.

The recent advances of AVISO data processing, combining multiple satellite altimeters operating simultaneously can provide an adequate characterization of the mesoscale dynamics. The spatial resolution (1/3°) of the AVISO data set is sufficient to compute geostrophic surface velocities and detect large-scale eddies. Sea Level Anomaly (SLA) and the corresponding geostrophic velocities are shown for the summer months in Figures 3 and 4. In early June, the Madeira Archipelago is surrounded by a large-scale cyclonic circulation as depicted in Figure 3a. This cyclonic circulation (C1) slightly decays toward the end of June and a positive SLA starts to emerge in the lee of Madeira Island by mid-July, Figure 3c. An anticyclonic eddy (A1) intensifies during August (Figure 4a) and remains roughly at the same position (32°N, 17°E) until mid-September (Figure 4c). Hence, the AVISO altimetry confirmed the presence of a coherent mesoscale anticyclone initially detected by the surface chlorophyll pattern. Remote sensing images of the Madeira wake have mainly detected the formation of cyclonic (cold core) eddies forming leeward of the south-west cape, i.e., "Ponta-do-Pargo" [*Caldeira et al.*, 2002].

3.2. Vertical Eddy Structure

In order to characterize the vertical structure of the anticyclone, 30 CTD profiles were taken along a 120 km transect. Figure 5 represents the locations of these vertical profiles with the trajectories for first 10 days of the four MLI buoys, launched on the 27 August 2011. These trajectories confirm the steady circular anticyclonic circulation depicted by the AVISO SLA data (Figures 4b and 4c). This analysis also corroborates that the first hydrographic transect crosses the eddy center. Figure 5 shows the positions of 24 UCTD (filled square) and 7 CTD (semifilled square) casts performed during the in situ survey (26–28 August 2011). Profile locations are plotted over the weekly trajectories of the iridium buoys. Gray circles note the launching positions of each drifter.

From these hydrographic measurements, cross sections of the vortex were extracted for further analysis (Figure 6). Density (sigma-t) and Brunt-Väisälä frequency plots are shown in Figure 6. The isopycnal downwelling within the anticyclonic core is around $\Delta h \simeq 100$m. According to the vertical stratification (see Appendix A),
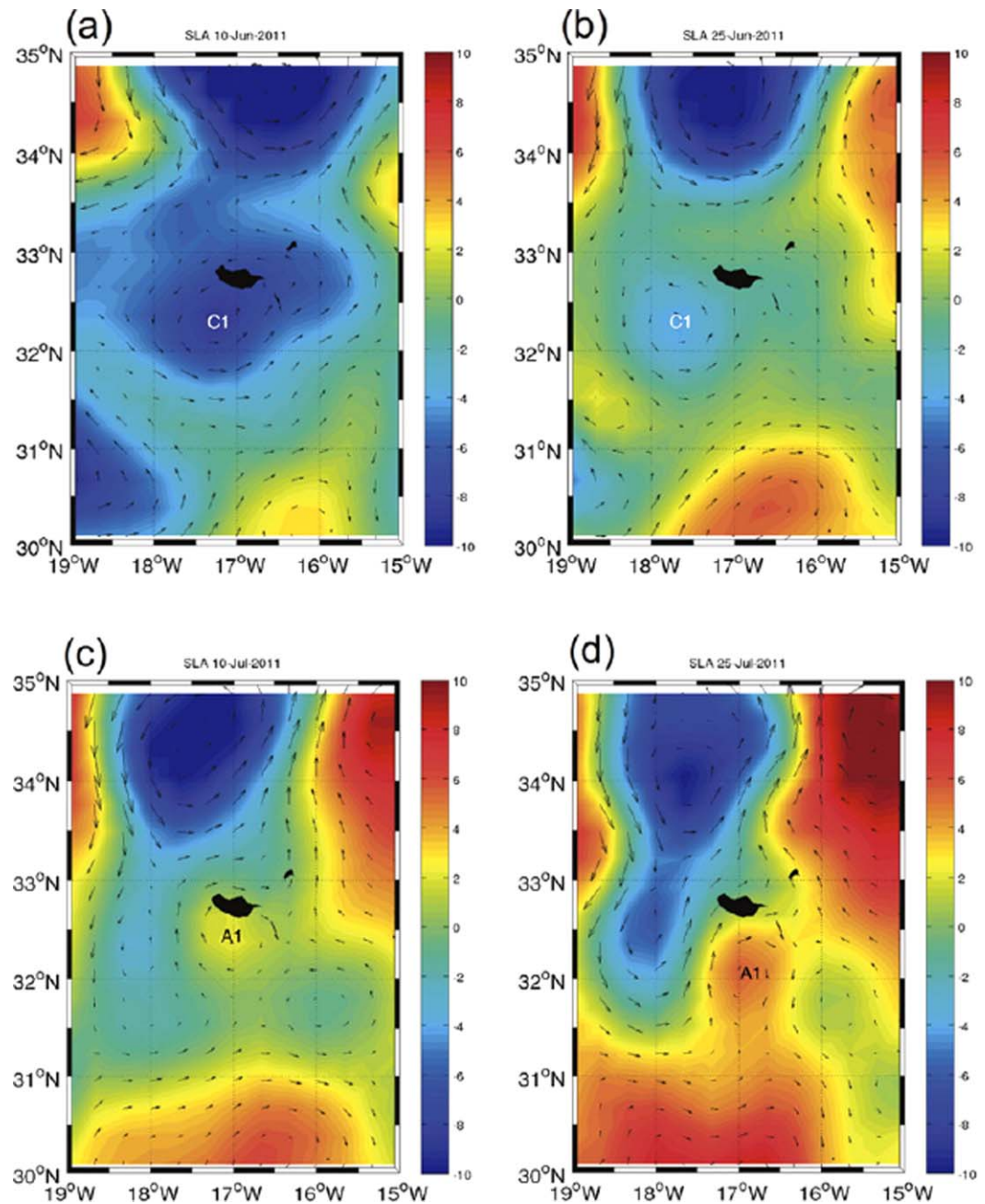
Figure 3. AVISO Sea Level Anomaly (SLA) and the corresponding geostrophic velocities (black vectors) for (a) 11 June 2011, (b) 25 June 2011, (c) 10 July 2011, and (d) 25 July 2011. The color bar of the SLA ranges from −10 to +10 cm.

the unperturbed thermocline depth is about $h = 100 - 120m$, whereas it could reach $h + \Delta h = 200m$ in the vicinity of the vortex center. Hence, the isopycnal downwelling induced by the anticyclone reaches a finite amplitude $\lambda = \Delta h / h \simeq 1$. For geostrophically balanced vortices, such a large isopycnal deviation could only be induced by an eddy that is large enough in comparison to the deformation radius (R_d) of the first baroclinic mode. In fact, according to the vertical stratification outside or inside the anticyclone we get $R_d \simeq 10 - 12km$, which is significantly smaller than the vortex size $R \simeq 30km$, estimated here from half the isopycnal deviation.

The isopycnical configuration shown in Figure 6, also denotes a lens-like shape located in the subsurface typical of intrathermocline eddies (ITEs). ITEs [*Dugan et al.*, 1982] are often anticyclones with a surface cap and have been found in several regions of the world oceans [*Kostianoy and Belkin*, 1989]. ITEs are also long-lived and retain much of the characteristics of their formation area. They frequently move far from their
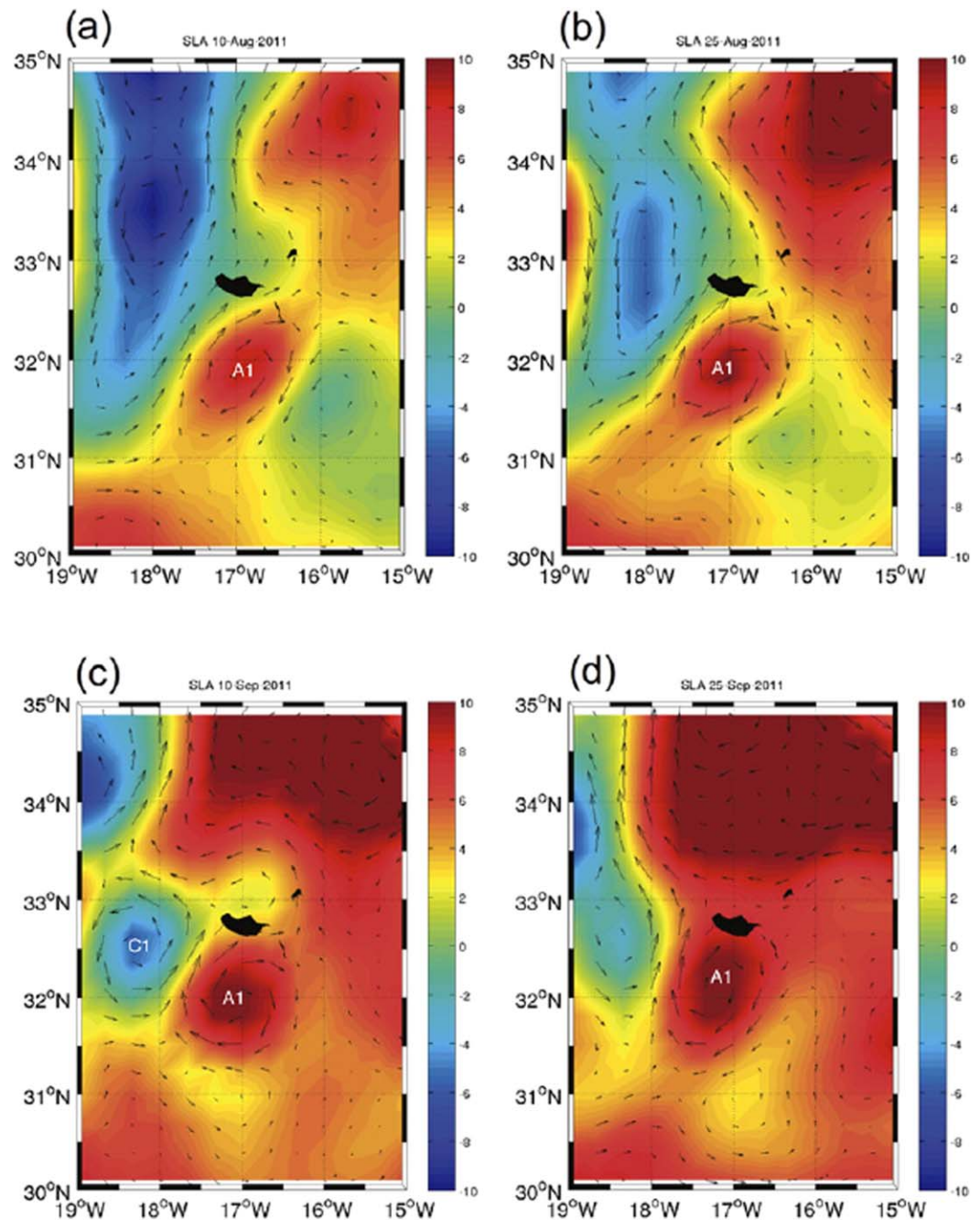
Figure 4. Same as Figure 3, for (a) 10 August 2011, (b) 25 August 2011, (c) 10 September 2011, and (d) 25 September 2011.

origin, becoming designated as MODE water eddies [*Nauw et al.*, 2006]. Atmospheric conditions responsible for the warm wake generation favor ITEs formation. Diabatic processes will reduce the potential vorticity (PV) when there is a net loss of buoyancy from the ocean to the atmosphere, depicted by the dooming of the isopycnals (see Figure 6). The buoyancy loss to the atmosphere triggers convective mixing, which reduces the stratification near the surface [e.g., *Marshall and Schott*, 1999]. Although ITEs have been sampled in many regions, their formation and earlier evolution has not been well documented. Notwithstanding, it is also true that different physical conditions can lead to the generation of ITEs, but the long-term monitoring of their generation sites can lead to further understand the dynamics of thermocline ventilation processes.
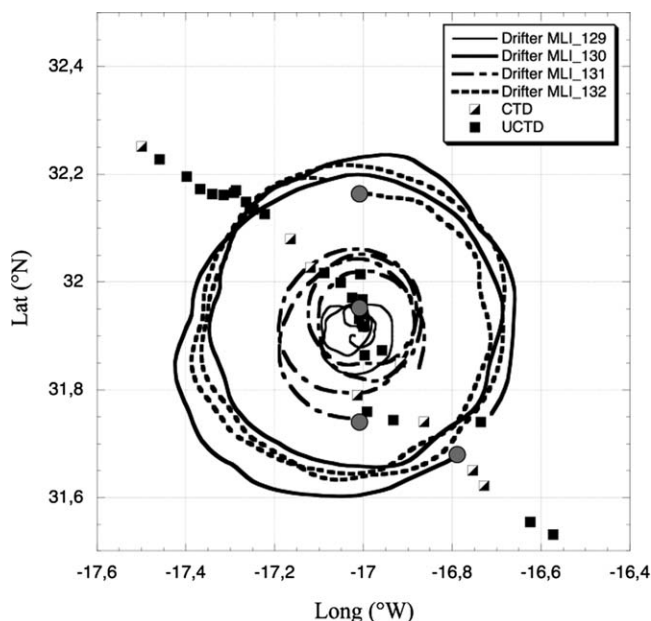
Figure 5. Positions of UCTD (filled square) and CTD (semifilled square) casts performed during the hydrographic survey (26–28 August 2011), plotted over the trajectories (lines) recorded by iridium buoys during the same week. Gray circles correspond to the buoys launching positions.
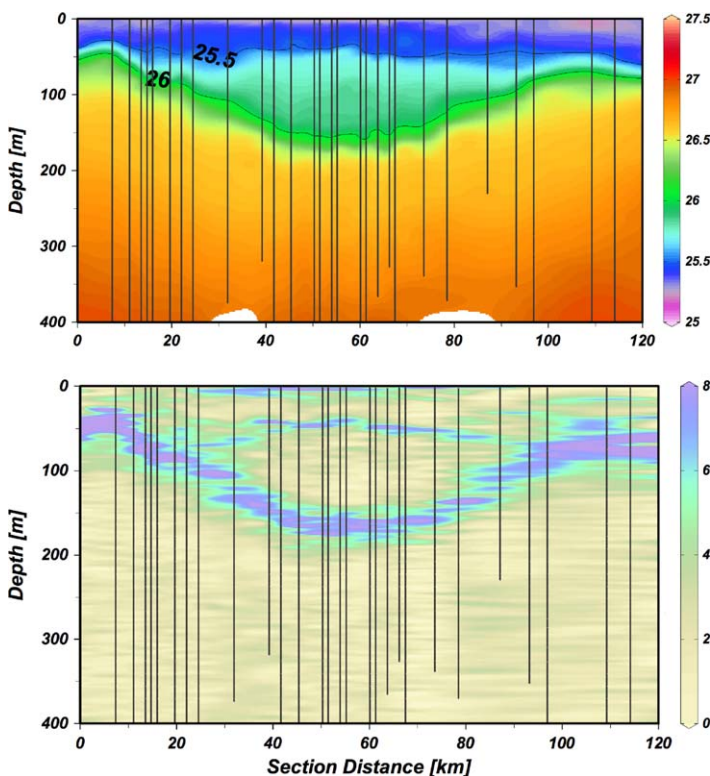
Coincidentally (or not), the Madeira MODE water has been detected by a permanent mooring located westward of Madeira (Kiel-276) [*Siedler et al.*, 1987]. The pycnostat was formed between 70 and 160 m during summer months, with temperature gradients varying between $17 - 18°C$ and density signatures of ≈ 25.5 kg m^{-3}. Hydrographic data from different cruises in the region estimated that the largest volumes of Madeira MODE water were formed during Spring and Summer months [*Siedler et al.*, 1987]. The authors also argued that Madeira MODE water was responsible for 15–20% of the volume of ventilated thermocline waters, in this density range, in the North Atlantic. Although this requires further investigation it is worth noting that anticyclones formed in the leeward side of Madeira, highly exposed to sea surface warming could become net contributors to the Madeira MODE water formation and/or to its long-range transport. *Sangrà et al.* [2009] analysis of historical altimetry data (1992–2006), showed several anticyclones forming leeward of all NE Atlantic islands (including Madeira), and propagating westward with lifespans of over 6 months.

Profiles of neutral density inside and outside the anticyclone does show the occurrence of a marked pycnostad inside the eddy (see Figure 7). Outside the eddy pycnocline occurs between ≈ 50 and 100 m, whereas inside the eddy the layer of less density changes (pycnostat) occurs between ≈ 50 and 150 m. T-S diagrams (not shown), identify the presence of the same water masses but depicted more (temperature and salinity) variability outside the eddy than inside, concurrently to what has been reported for other ITEs [*Gordon et al.*, 2002; *Nauw et al.*, 2006; *Hogan and Hurlburt*, 2006].

Figure 6. (top) Vertical transect of density (sigma-t, in kg m^{-3}). (bottom) Brunt-Väisälä frequencies (N, in cycl h^{-1}) across the anticyclonic eddy. The black vertical lines correspond to the vertical profiles performed during the hydrograhic survey (26–28 August 2011) shown in 5.
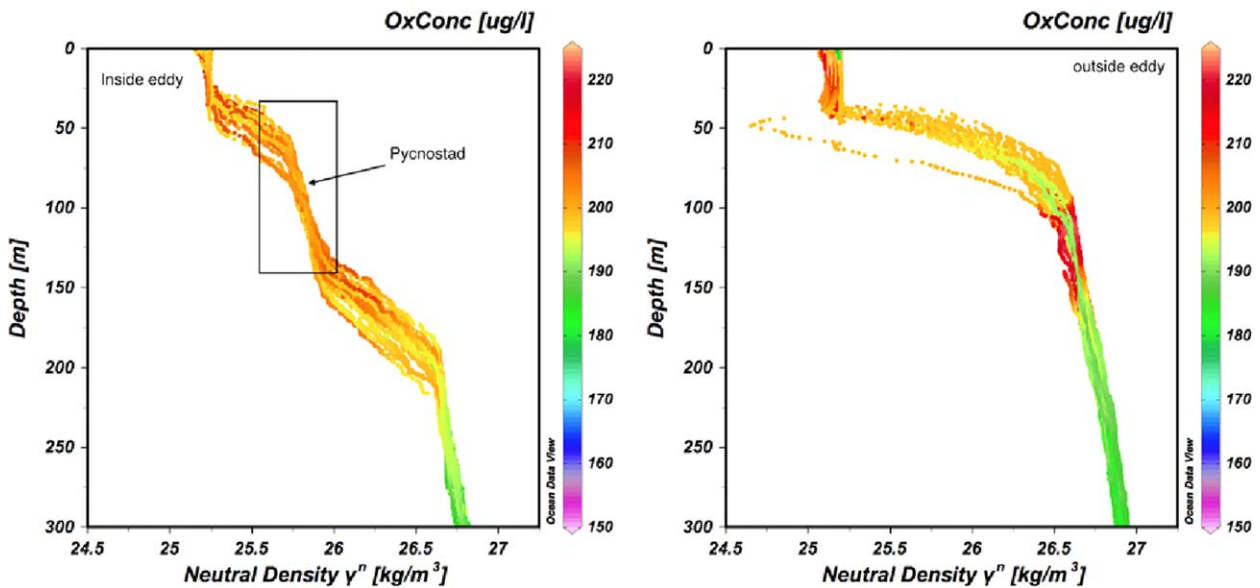
Figure 7. Profiles of neutral density calculated from CTD data extracted from stations located (left) inside and (right) outside of the eddy.

Using the hydrographic data, it was also possible to calculate the perpendicular components of the geostrophic flow, which have confirmed the occurrence of an anticyclonic motion down to at least $\approx$300 m depth (Figure 8). Geostrophic velocities were derived from the dynamic height differences between each two stations, thus the squares shown in Figure 8 represent the midpoint between stations. A level of no motion at 500 m was considered and all stations used for the calculation had measurements from top to bottom. A piecewise linear least squares analysis was used to determine the depth ranges with significant difference in order to proceed with meaningful calculations. Velocities at the surface reached mean values of 0.5 ms^{-1}, whereas at depth ($\approx$200 m) were lower than 0.1 ms^{-1}.

3.3. Dynamical Analysis of the Eddy Velocity Profile

In order to characterize the radial velocity profile of the anticyclone, we first used the velocity measurements derived from the motion of MLI-buoys. From the drifter trajectories plotted in the eddy frame we extracted for each successive position $(X(t), Y(t))$ the radial distance $R(t)$ from the drifter to the eddy center. Specific time intervals where the drifters trajectories remain almost circular were considered. Figure 9a shows the mean radius R_i, for several loops(i), as a function of the mean azimuthal velocity (V_i). The intermittent local wind stress or the small-scale wave activity induces dispersion in the drifter dynamics and a wide range of R_i values are explored while the four drifters loop inside the eddy. The maximal eddy velocity $V_{max} \simeq 50$cms^{-1} is reached for the characteristic radius $R_{max} \simeq 25$ km and taking into account $f = 2\Omega_0 sin\theta_0 \simeq 0.77 \times 10^{-4}$s^{-1} the local Coriolis parameter at the eddy latitude $\theta_0 \simeq 31.9°$N, results in a vortex Rossby number $Ro = V_{max}/(fR_{max}) \simeq 0.26$ of this anticyclone during September–October. This moderate value of Ro shows that the centrifugal force is relatively small in comparison with the Coriolis force and the circular eddy complies with the geostrophic balance assumptions.

According to standard dimensional analysis, the horizontal pressure gradient for an equivalent two-layer model, scales as $\partial_r p \sim \Delta \rho g \triangle h \sim \rho \lambda g^* h$, where $g^* = (\triangle \rho / \rho)g$ is the reduced gravity and λ represents the relative deviation of the upper layer (the surface layer above the thermocline). The local vortex Rossby number and the isopycnal downwelling of circular anticyclones should then follow the relation:

$$Ro \sim \lambda (\frac{R_d}{R_{max}})^2 \qquad (1)$$

with $R_d = \sqrt{g^*h}/f$. Hence, the geostrophic relation gives $\lambda \simeq 0.96$ when $Ro \simeq 0.26$ and $R_d/R_{max} = 0.52(Bu = 0.27)$, which is in good agreement with the value $\lambda \simeq 1$ deduced from the hydrographic transect data set. We can also estimate the core vorticity of this anticyclone from the angular rotation $\omega(r) = v(r)/r$. The vorticity in cylindrical coordinates is given by:
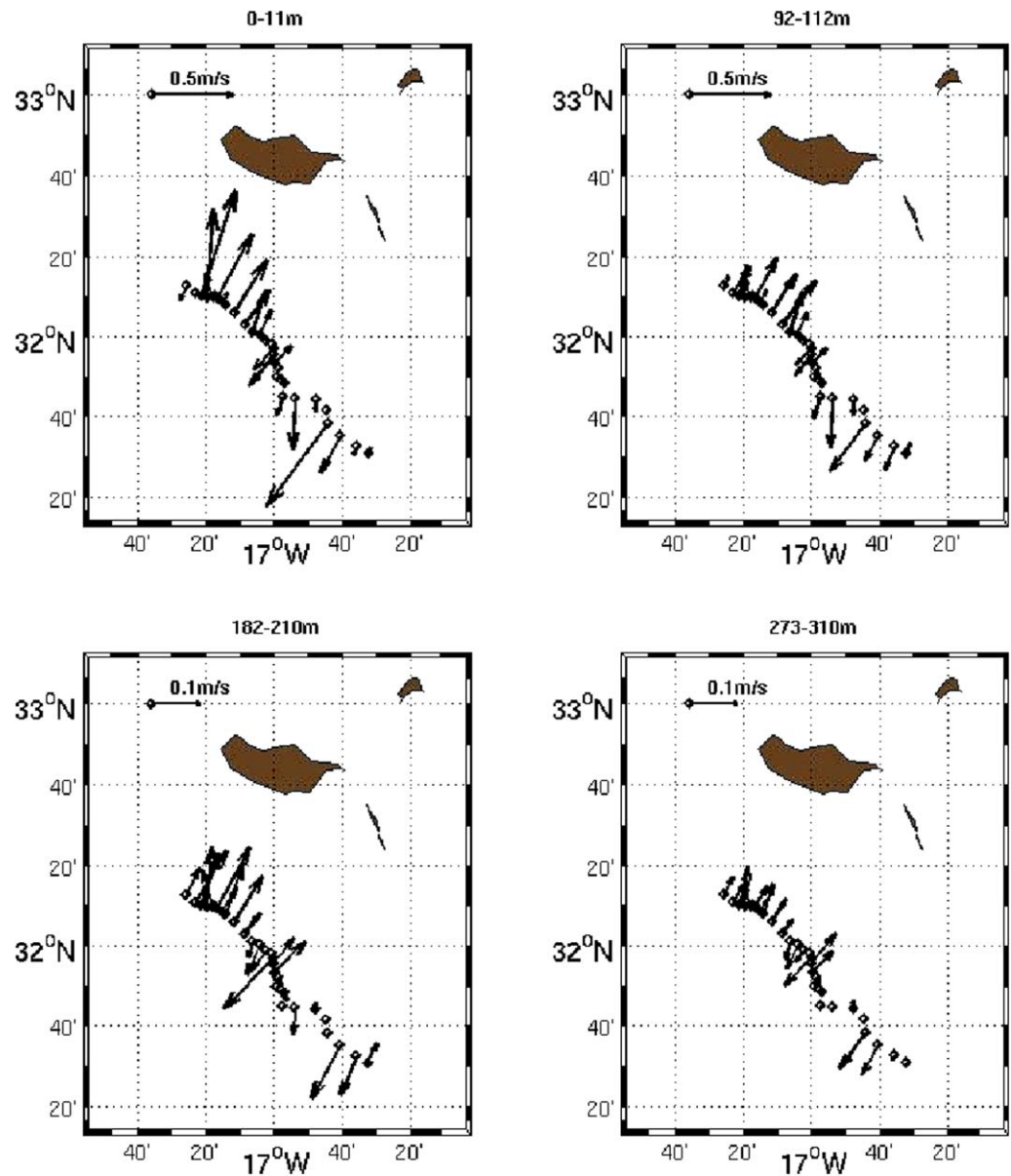
Figure 8. Geostrophic velocities computed at different depth intervals from the transect represented in Figure 6.

$$\zeta(r) = \partial_r v(r) + \frac{v(r)}{r},$$

(2)

and therefore, according to a standard Taylor expansion at the center, the relative vorticity becomes:

$$\frac{\zeta}{f}(r \simeq 0) \simeq 2\frac{v}{fr}(r \simeq 0) = 2\frac{\omega(0)}{f}$$

(3)

which is directly proportional to $\omega(0) = -0.54 \times 10^{-4} s^{-1}$, calculated from the local slope of the azimuthal velocity profile at the origin (solid line in Figure 9a). The relative core vorticity of this anticyclonic eddy is finite $\zeta/f = -0.7$ but it remains below $-f$. For such range of parameters, this mesoscale anticyclone cannot be affected by unstable inertial perturbations and could therefore remain stable and coherent for several months [*Kloosterziel and van Heijst*, 2006; *Carnevale et al.*, 2011; *Lazar et al.*, 2013a, 2013b].
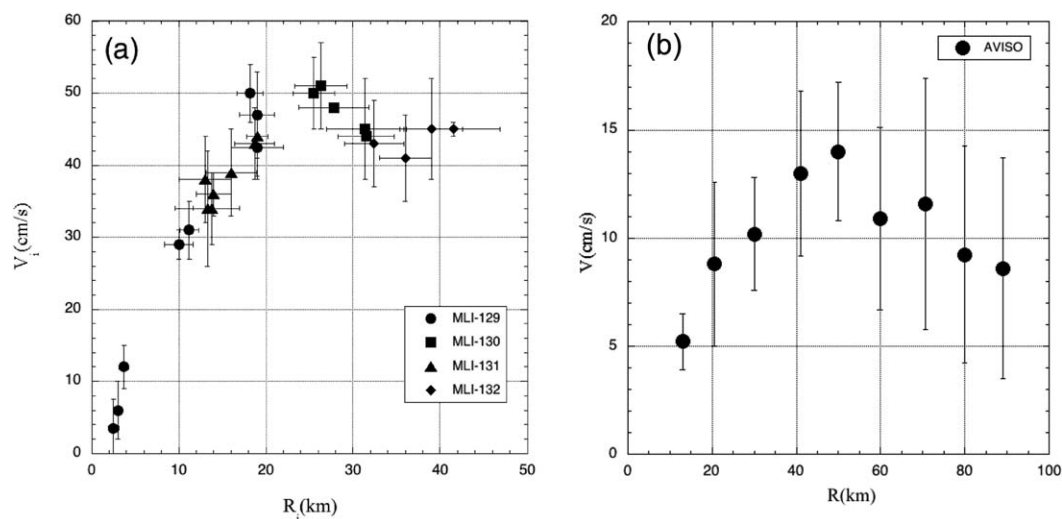
Figure 9. Amplitude of the azimuthal velocity profile of the anticyclone estimated from: (a) buoys trajectories with a drogue at 50 m, and from (b) AVISO geostrophic velocities during August and September 2011. The solid line in Figure 9a corresponds to the linear fit $V(r) = \omega(0)r$ in the vortex core.

On the other hand, the geostrophic velocities computed from the AVISO SLA lead to a circular velocity profile (Figures 3 and 4), which corresponds to a weaker ($V_{max} \simeq 14\text{cm s}^{-1}$) and larger ($R_{max} \simeq 40-50\text{km}$) anticyclone. The corresponding vortex Rossby number is therefore much smaller $Ro \simeq 0.06$. It is expected that the geostrophic velocities computed from the coarse resolution ($1/3°$) AVISO data will under estimate the intensity of small surface vortices having a radius close to the AVISO resolution. Therefore, the quantitative significance of such satellite-based measurements should be considered with care for small wake eddies.

3.4. Eddy's Interior Sampled at High Resolution

Once the eddy center was accurately identified from the buoy trajectories, the G2 Slocum glider was deployed in the lee of Madeira island, a few weeks later (from 12 to 29 September 2011). The analysis of the surface drifters provided the real time positions of the anticyclone and its trajectory. Hence, in collaboration with the "Division Technique" of the French "Institut national des sciences de l'Univers (INSU)" team and the EGO (Everyone's Gliding Observatory) network (http://www.ego-network.org) we were able to optimize the glider navigation, redefining waypoints and the glider trajectory on a daily basis. The synoptic sampling of a mesoscale eddy using a glider was a challenging task, since a full 100 km long transect could take more than a week to complete, considering the relatively slow glider navigational speed ($\approx 0.34\text{ ms}^{-1}$). The fact that the eddy was relatively close to the island and did not drift over long distances during the sampling, and considering that most of the navigation took place in the sheltered leeward region, it enabled the glider to accomplish two very high resolution transects across the eddy. In comparison, the in situ survey using the R/V took <2 days to complete one eddy-crossing, (Figure 6, 30 casts over ≈ 100 km transect), whereas the glider performed over 200 casts per transect. The entire glider survey is plotted in the island frame in Figure 10a. Transect-1 (Figure 10b) and transect-2 (Figure 10c) are plotted in the moving eddy frame where (X,Y) correspond to the relative glider distances from the vortex center. The transect-1 successfully crossed the center of the anticyclone, while in transect-2 the glider was deviated by an opposing circulation. Nevertheless, both transects provided a very high resolution sampling of the eddy relatively to the ship or satellite-based measurements (≈ 500 m on the horizontal and ≈ 1 m on the vertical), allowing for a more detailed characterization of the vortex structure, including some suggestions for its internal and biological activities.

According to Figures 11b and 12b, the anticyclone is characterized by a strong downwelling of the isopycnal layer below $\sigma = 26\text{kg/m}^3$, while the thickness of intermediate layers increased significantly ($25.5\text{kg/m}^3 > \sigma > 26\text{kg/m}^3$). The vortex circulation did not modify the thickness of the surface mixed layer, which remained at 50 m. An identical signature was found in the hydrographic section during the CTD/UCTD campaign, as shown in Figure 6. The depth of the isopycnal layer $\sigma = 26\text{kg/m}^3$ varied from 60 to 70 m outside
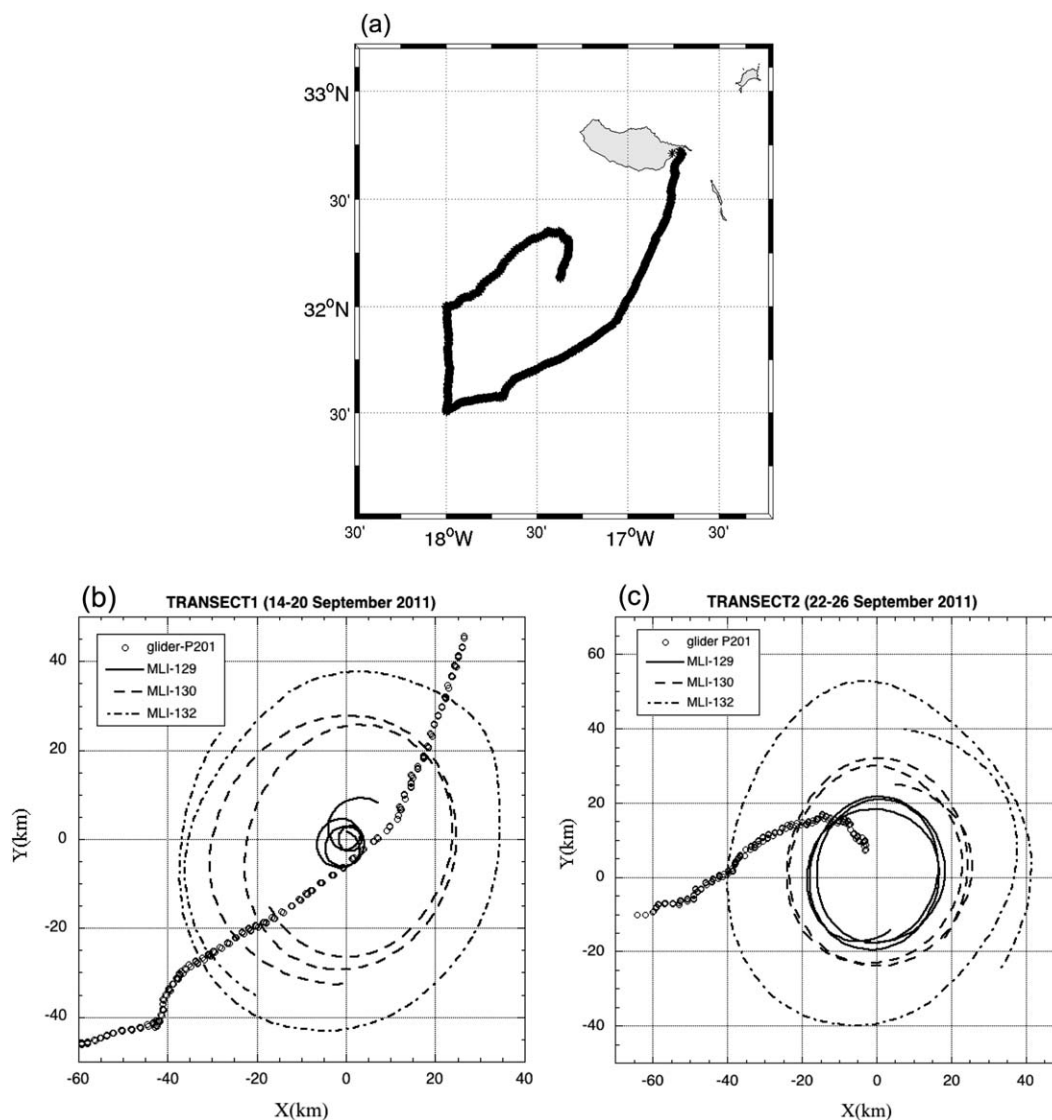
Figure 10. Trajectory of the G2 glider South of Madeira island (a) from the deployment 12 September 2011 to the recovery 29 September 2011; (b) trajectories of the glider and three iridium buoys for the transect-1; (c) transect-2 is plotted in the drifting eddy frame. The center ($X = 0$, $Y = 0$) of the anticyclonic eddy was calculated from the analysis of the four drifter trajectories. The glider transect-1 was accomplished in 6 days, while transect-2 was completed in 4 days.

of the vortex, reaching 160 to 180 m in its core. The comparison between the two density sections, Figures 6 and 11, confirms that the three-dimensional structure of this anticyclone did not change significantly from August to September. Neither wind-induced forcing nor inputs of water masses modified its internal structure during this period as verified by the T-S analysis carried out on the CTD data (not shown).

However, the high resolution measurements provided by the glider exhibit small-scale oscillations of the isopycnals which cannot be detected by coarser resolution of the CTD/UCTD ship campaign. As can be seen in Figures 11 and 12, the amplitude of these isopycnal fluctuations can reach an amplitude of few tens of meter, besides, the oscillations of the isopycnal depth and the intensity of the Deep Chlorophyll Maximum (DCM) seems to be strongly correlated. These submesoscale fluctuations are most probably the signature of inertia-gravity waves generated by the local wind forcing. Recent studies of *Kunze* [1985, 1986] have shown that amplification of near inertial waves is typical for anticyclones when the relative vorticity becomes finite. *Snyder et al.* [2007] have also shown that for a dipolar structure, the internal wave amplitudes tend to be amplified in the anticyclonic partner.
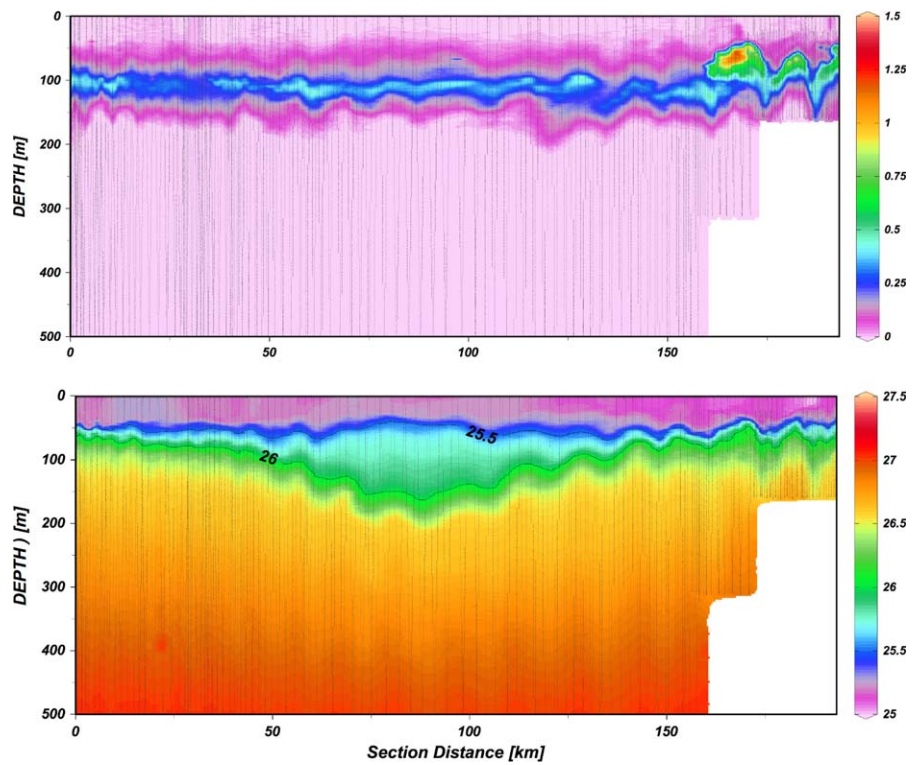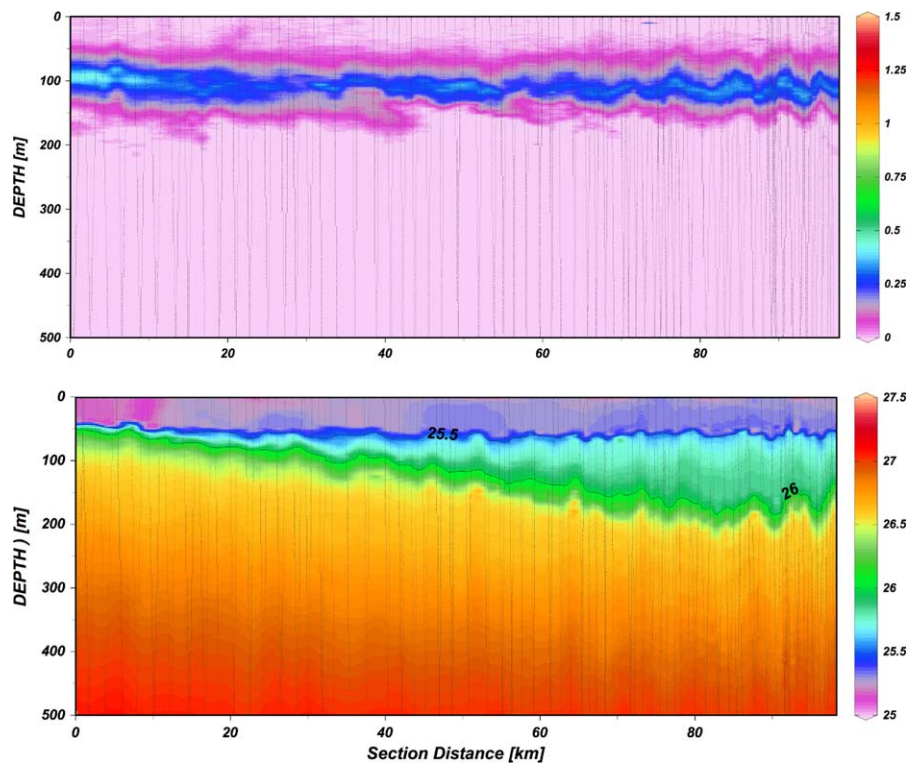
Figure 11. Glider high resolution measurements of (top) chlorophyll concentration (mg m^{-3}) from fluorescence measurements and (bottom) density (sigma-t, kg m^{-3}) along transect-1, see Figure 10, for sampling trajectory.
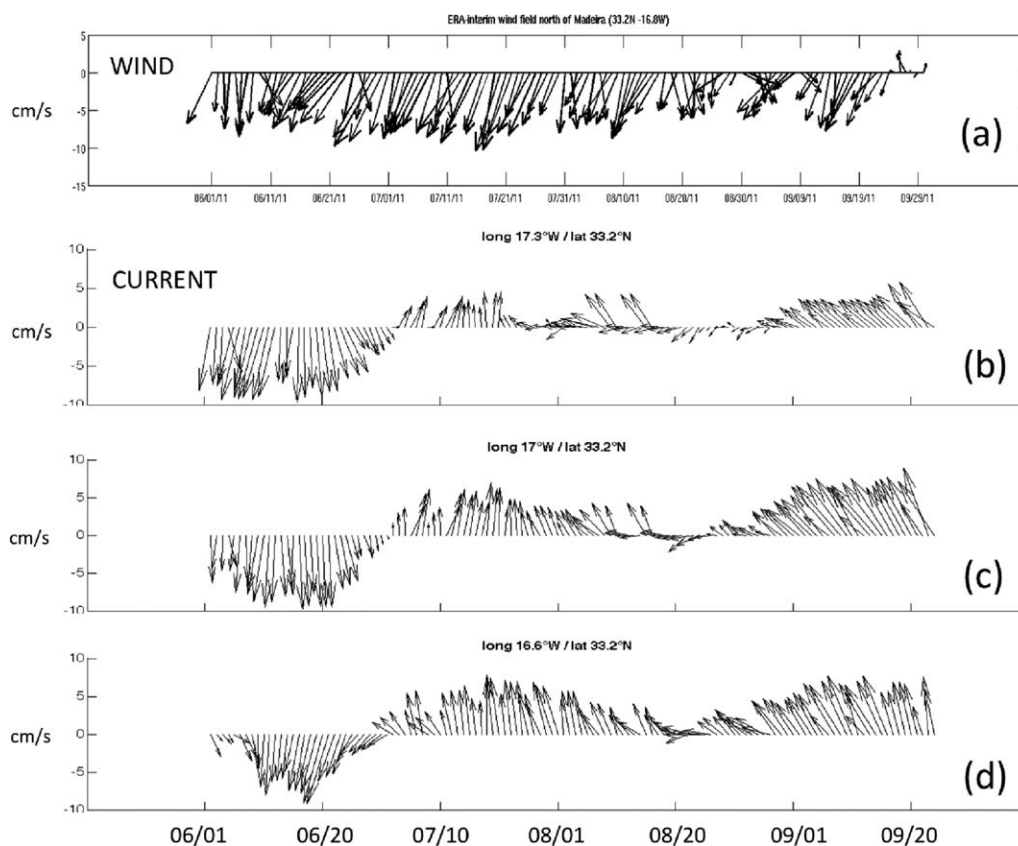

Figure 12. Glider high resolution measurements of (top) chlorophyll concentration (mg m^{-3}) from fluorescence measurements and (bottom) density (sigma-t, kg m^{-3}) along transect-2, see Figure 10, for sampling trajectory.

Figure 13. Time-series of (a) incoming winds; and (b–d) geostrophic currents in a windward latitude (33.2°N). Geostrophic currents were extracted from three locations in the same zonal transect: (b) 17.3°W; (c) 17°W; and (d) 16.6°W.

Another interesting result obtained from the glider measurements was the fact that this significant isopycnal downwelling at the eddy core had no impact on the deep chlorophyll maximum, represented here by fluorescence measurements (Figures 11 and 12). The DCM oscillates around a mean averaged level of $100 - 110$ m along both transects with no significant changes occurring inside the eddy. The most significant increase in the chlorophyll concentration was observed near the coast during the first part of transect-1 (the glider deployment area), probably due to the strong internal wave activity and/or by the localized upwelling often induced by an underwater promontory which connects Madeira with the Desertas islands [*Caldeira et al.*, 2002]. The uniform mean DCM depth inside the anticyclone also suggests that the vertical advection triggered by the initial stages of the vortex formation occurred sometime prior to the glider sampling.

MODE water eddies have been suggested to enhance eddy-upwelling and provide small but steady pulses of nutrient supply to the euphotic zone, which ultimately allows the sustenance of large phytoplankton cells for extended periods [see *McGillicuddy et al.*, 2007; *Bibby et al.*, 2008, for details]. It is possible that by capturing the ITEs in such an early stage of its development there was not enough time for significant biological growth to take place.

3.5. Evidences of a Wind Generated Event
According to the analysis of the AVISO altimetry data the first signature of the anticyclonic eddy in the South of Madeira appeared in mid-July (Figure 4c). This anticyclone was not detected in the area during the preceding weeks, which was dominated by a regional cyclonic circulation at the surface. Its generation appears to be an oceanic response to the island perturbation of the atmospheric flow, i.e., wind curl. In order to determine the dominant forcing, we concurrently analyze in Figure 13 the temporal evolution of the wind and oceanic geostrophic currents, in the north (windward) side of Madeira, from June to September 2011.
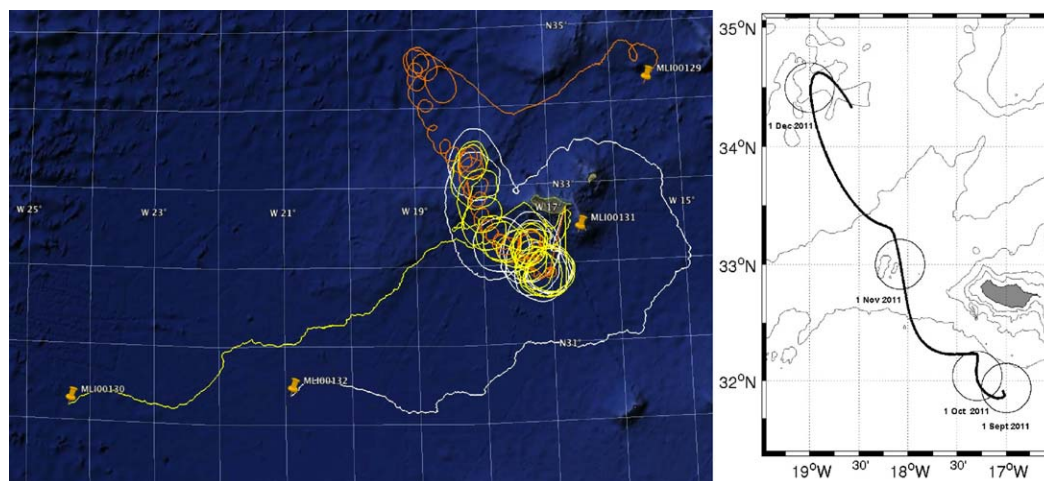
Figure 14. (left) Full trajectories of the four buoys from 26 August 2011 to 10 January 2012. (right) Trajectory of the eddy center from 1 September 2011 to 10 December 2011 computed from a reanalysis of the four drifters trajectories. A 50 km circle (right) indicates the monthly position of the anticyclone.

Regrettably, we did not have the means to perform any oceanic in situ current measurements and we can only rely on the geostrophic velocities computed from the AVISO altimetry to estimate the incoming oceanic flow in this region. Nevertheless, even if the geostrophic velocities may underestimate the flow amplitude, we are confident that the mean orientation of the surface circulation measured with satellite altimetry is realistic, after all the AVISO data was successfully used to locate, sample and monitor an anticyclone occurring leeward of the island. The temporal evolution of velocity vectors, located at the longitudes (17.3° W; 17°W; 16.6°W) and at the same upstream latitude 33.2°N are represented in Figure 12. One of the most noticeable results is that the weak oceanic flow is mainly directed toward the north, during July, August, and September. This somewhat invalidates the hypothesis that the flow-bathymetry interaction is solely responsible for the generation of mesoscale eddies appearing in the leeward side.

In absence of a meteorological station measuring unperturbed flow in the windward side the island, the upstream wind amplitude and direction was extracted from the ERA-interim reanalysis data set at the grid point (33.2°N, 16.8°W) (Figure 13a). North and north-east winds, were present for all the summer season, with an amplitude varying from 5 to 15 ms^{-1}, while the strongest winds occurred from mid-June to mid-July. According to the high-resolution WRF-ROMS simulations performed by *Couvelard et al.* [2012], the wind stress curl induced by the island orography generates an oceanic vortex street when the mean upstream winds exceed $10 - 15$ ms^{-1}. Even if this study focus on the summer 2008, similar values were resolved by the 2011 ERA-interim data set, just a few weeks before the eddy was first detected. In addition, the initial location of the anticylcone (Figure 4c) coincides with the generation area identified in the the WRF-ROMS study [*Couvelard et al.*, 2012, Figure 16]. Hence, the large mesoscale eddy formed in July 2011 in the lee of the island is an ocean response to the wind-forcing mechanism and not the consequence of the incoming flow interacting with the bathymetry.

3.6. Long-Term Evolution

An unusual aspect of this anticyclone occurring leeward of a small island was the fact that it stayed in position (around 32°N, 17°W) for 10 weeks after its initial detection (10 July to 25 September). However, the anticyclone is not an isolated event and we should also consider the interaction with the cyclonic circulation located at the South-West of Madeira (32.5°N,18°W), visible (C1) in Figures 3d and 4. Indeed, the coupling of this cyclonic circulation with the wind-induced anticyclone lead to a dipolar structure, which should promote a northward drift (or to the northeast) but the anticyclone stays blocked by the coasts of Madeira and the Desertas islands. This specific configuration may explain the quasi-steady position of the anticyclone for several weeks. In general, the displacement of coherent vortices is a function of the planetary and topographic beta-effect, large-scale geostrophic circulation, Ekman drift, and self-propagation depending on the vortex vertical structure [see for instance *Morel and McWilliams*, 1997]. Nevertheless, in the absence of significant oceanic advection, the Beta-effect, and the net Ekman transport resulting from the persistent NE trade winds
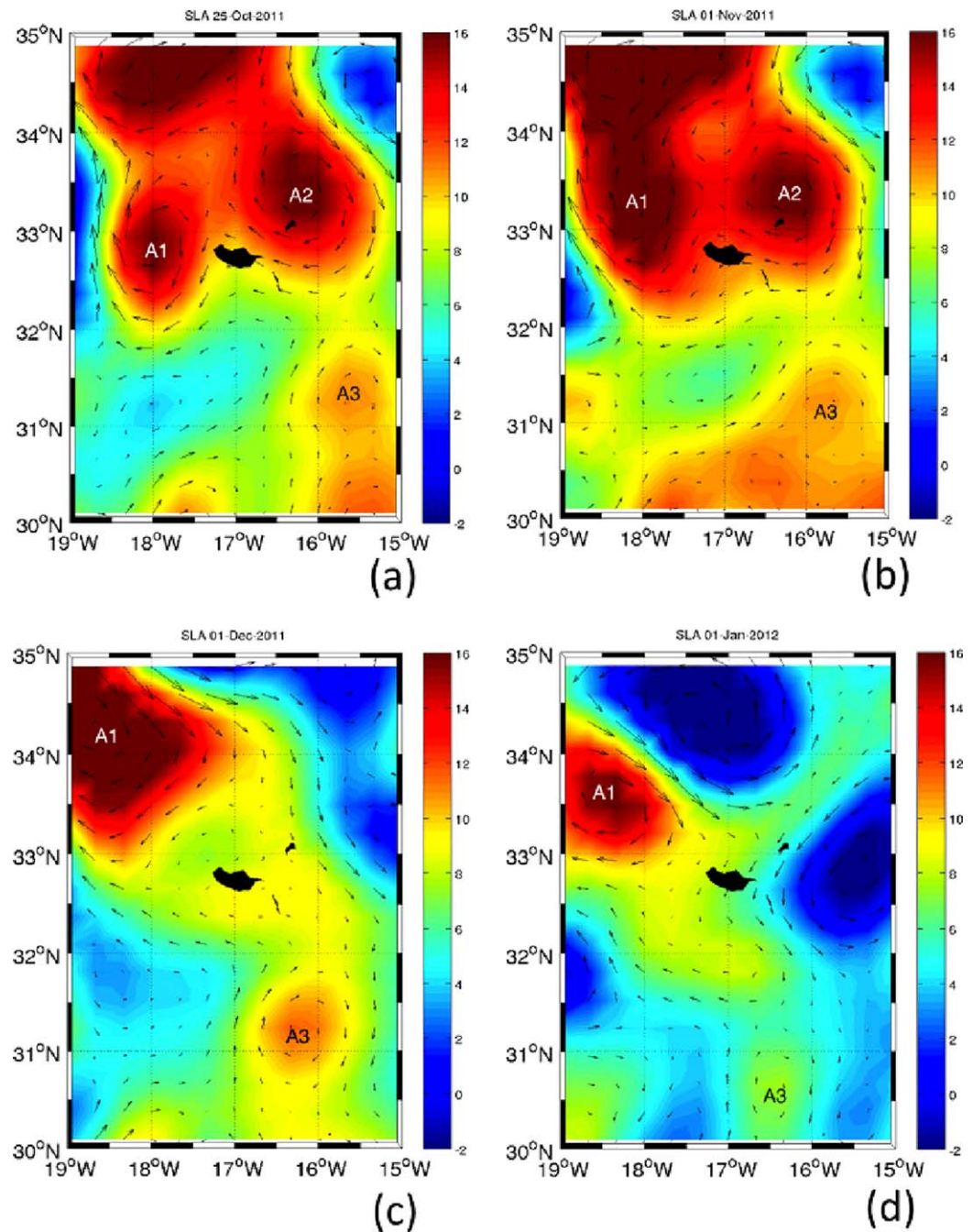
Figure 15. AVISO SLA and the corresponding geostrophic velocity field (black vectors) for the (a) 25 October 2011, (b) 1 November 2011, (c) 1 December 2011, and (d) 1 January 2012. The color bar ranges from −2 to 16 cm.

should both contribute to a slow westward (or northwestward) drift of the anticyclone [*Morel and Thomas*, 2009]. Hence, the cyclone slightly move toward the northwest in October and it takes a relatively long time for the anticyclone to escape from the island shelter (Figure 14) with its cyclonic partner. The eddy center moved diagonally from 32°N to the 34.5°N latitude, before merging with other regional structures (after 3 months), loosing its identity in the altimetry data (Figure 15). If we consider that in 3 months the eddy traveled 450 km, this results in an eddy translation speed of about ≈5 km/d (≈ 6 cm s^{-1}). For this specific 2011 event, the long term northwestward trajectory of the anticyclone started close to the islands, which differed slightly from previous numerical results [*Couvelard et al.*, 2012], which suggested that the leeward eddies might travel southward for some time, before drifting westward (and/or northwesterly). Thus, we hypothesize that
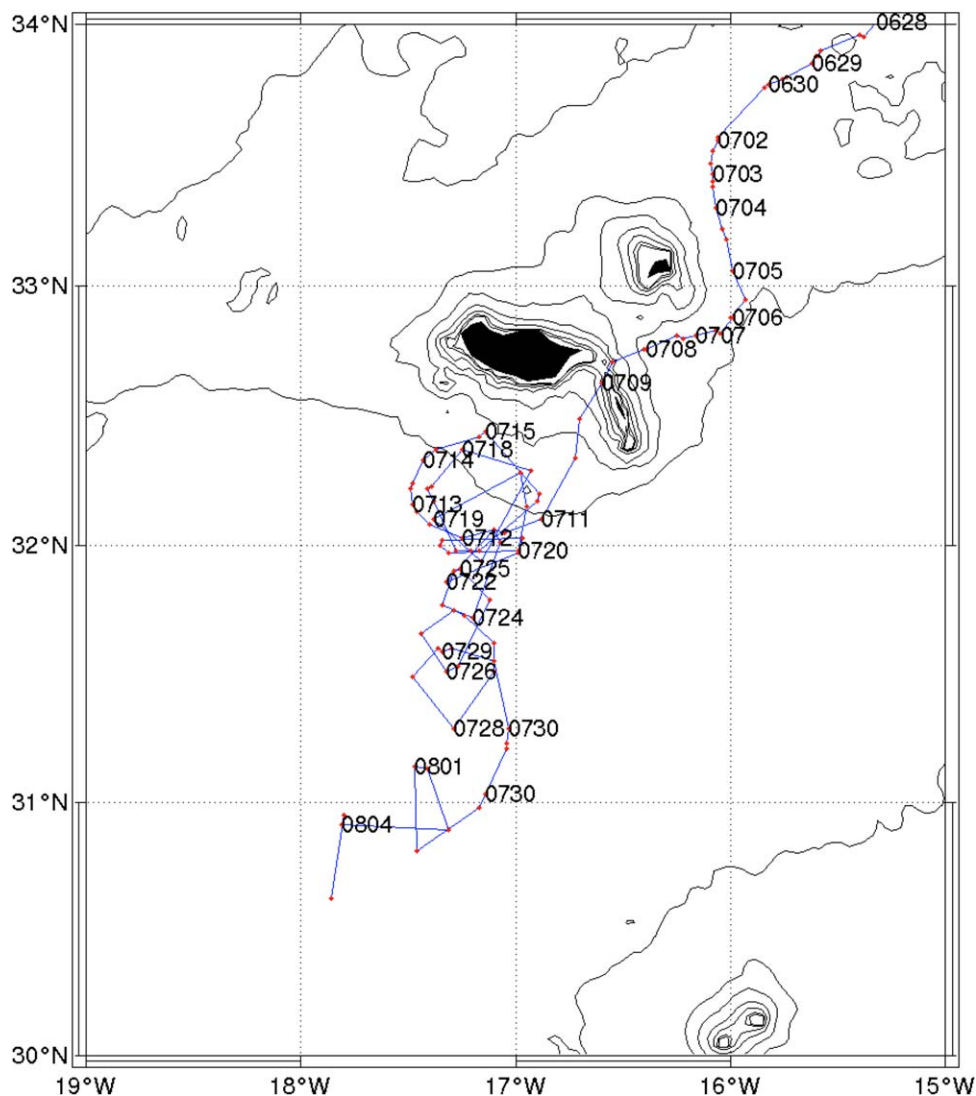
Figure 16. Trajectory of an SVP buoy, captured by an anticyclonic eddy motion leeward of Madeira Island, between the 11 July and 4 August 1994.

depending on the strength of the atmospheric wakes (e.g., atmospheric stratification; wind speed and direction; etc.), and consequently on the wind shear formed leeward of the island flanks, and depending on the neighboring ocean circulation (e.g., dipoles; south-north currents, etc.), oceanic eddies might escape the island influence at different distances from the coast. This is an issue that can lead to several shedding scenarios and that should be investigated in future works.

A sequence of altimetry data (Figure 15) shows the northwest drift of the anticyclone, depicted by the SLA and geostrophic velocity fields. It also shows, the occurrence of another incoming anticyclonic eddy (A2), i.e., not locally generated, in
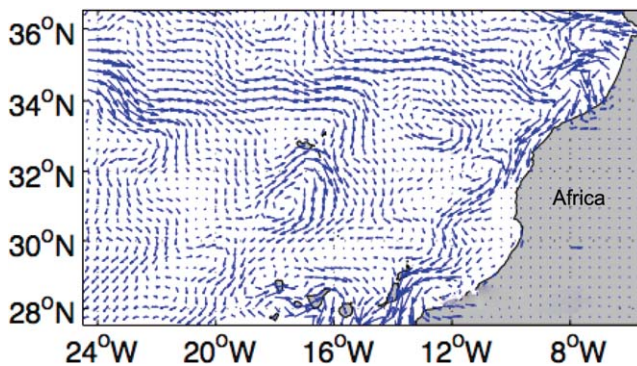
Figure 17. Summer climatology (July–September) of geostrophic currents derived from AVISO data, from 1992 to 2010 for the Madeira NE Atlantic region.

late October and early November. In comparison, the incoming eddy due to its size and position relative to the islands, was deviated by the archipelago and drifted southward, disappearing from our study region within a month. As in laboratory experiments [*Cenedese*, 2002; *Adduce and Cenedese*, 2004; *Cenedese et al.*, 2005], the incoming anticyclonic eddy generated a streamer around the archipelago (anticyclonic buoyant flow), after interacting with the island. Conservation of circulation around an island [*Godfrey*, 1989; *Pedlosky et al.*, 1997] suggests that these streamers arise because dissipation generated where the eddy impinges on the island must be balanced by dissipation elsewhere along the island perimeter [see also *Andres and Cenedese*, 2013].

3.7. Historical Evidences

After confirming the formation of an antiyclone, leeward of Madeira, there was a need to learn more about its reoccurrence in the historical records. *Martins et al.* [2002], studied the near-surface circulation using SVP drifter trajectories, as part of the WOCE-TOGA study of the eastern North Atlantic including the Iberian Peninsula, the Azores, and the Canary Islands. Although not specifically mentioned in the discussion two of the drifters found their way south, passing between Madeira and Desertas Islands, getting caught in an anticyclonic motion, leeward of the island. The first anticyclonic motion detected with the SVP drifters was observed between the 9 and 30 of July 1994 (Figure 16), whereas the second event took place between the 15 September and the 10 October 2007. The trajectories of SVP drifters with a "holey-sock" centered at 15 m (inside the summer mixed layer) are strongly influenced by the wind forcing but did not remain trapped for a long time within the vortex core. As shown in Figure 16, the SVP buoy trajectory describe anticyclonic loops for less than a month but the underlying anticyclonic vortex could remain coherent for a much longer time. Hence, the generation of an intense mesoscale anticyclone during the summer 2011 in the south of Madeira is not an isolated event.

In addition, analyzing historical (1997–2011) altimetry data produced by AVISO, it is possible to distinguish the predominance of an anticyclonic geostrophic motion, leeward of Madeira Island, particularly during the summer months (Figure 17). The mean summer circulation takes the proportion of a small gyre including the leeward region of Madeira and reaching as south as the Selvage Islands. Even the AVISO data set may not fully resolve the size and the intensity of small-scale island wake eddies a positive SLA signature induced by frequent eddies should be detected. Hence, this mean anticyclonic motion, which occurs in the SE leeward region could be due to the reoccurrence of long-lived anticyclones during summer months.

4. Conclusions

This study is the first clear evidence of the formation of a mesoscale anticyclone leeward of Madeira. A multiplatform approach, combining in situ survey and remote sensing analysis was needed to identify the vortex formation and quantify accurately its dynamical parameters. Due to the formation of warm wakes in the lee of mountainous islands passive satellite sensor data must be complemented with altimetry and in situ data in order to detected and monitor the evolution of mesoscale coherent structures.

The typical radius ($R_{max} \simeq 25$ km) of this oceanic anticyclone exceeds the local deformation radius (Rd $\approx$ 10–12 km) and scales with the mean island radius. With a maximal azimuthal velocity $V_{max} \simeq 50$cm s^{-1}, the vortex Rossby number remains moderate ($Ro = V_{max}/(fR_{max}) \simeq 0.26$) even if the relative core vorticity reaches a finite value $\zeta/f = -0.7$. The formation of such a large and intense vortex in less than a month is explained by the oceanic response to the winds modified by the island orography. As suggested by the high resolution WRF-ROMS simulations performed by *Couvelard et al.* [2012] the wind stress curl induced by the high island orography could generate oceanic vortices without any upstream oceanic currents. When the anticyclone was formed in July–August 2011 the oceanic flow was opposite to the wind direction, and therefore, cannot contribute positively to the generation process. Hence, this survey confirms *Couvelard et al.* [2012] simulations, i.e., the wind is a major mechanism for eddy generation in the lee of Madeira, particularly during summer months.

This wind-induced anticyclone has an unusual long residence time near the island (10 weeks). When it escapes from the island influence, the eddy traveled about 450 km northwesterly against the predominant winds, in response to the net Ekman transport and to a dipole structure. Hence, the spatiotemporal

variability of the wind forcing and the oceanic flow seems to prevent the formation of a standard Karman vortex street in the lee of the Madeira Archipelago. Nevertheless, some historical records indicate that the 2011 event is not isolated and few other drifters were trapped, during summer months, within anticyclonic structures in the same location. At regional scale, a mean anticyclonic gyre seems to dominate the summer climatology in the SE of Madeira.

Another important aspect to note about this anticyclone is that it assumed an intrathermocline configuration, caped at the surface by a warm water wake. MODE water eddies are the long-range expression of ITEs, and western of the island Madeira Mode Water has been previously detected. Thus, future works should continue to investigate the link that might exist between long-lasting ITEs formed in the lee of Madeira, thermocline ventilation and the transport of Madeira MODE water across the Atlantic Basin. Future analysis should also consider its interannual variability and its impact on the long-range transport of pollutant or biogeochemical species.

Appendix A: Estimation of the First Baroclinic Deformation Radius

For a continuous stratification $\rho(z)$, the linear eigenmodes and the corresponding deformation radius are given by the equation:

$$\partial_z \left(\frac{\rho_0 f^2}{g} \frac{\partial_z \psi_n}{\partial_z \rho} \right) = \partial_z \left(\frac{f^2}{N^2(z)} \partial_z \psi_n \right) = -\frac{\psi_n}{R_{d,n}^2} \tag{A1}$$

where $R_{d,i}$ are the deformation radius associated to the baroclinic modes $n = 1, 2, \ldots$ and $\partial_z \psi_n(z = 0) = \partial_z \psi_n(z = -H) = 0$. This equation is identical to eqn. (5.204) in *Vallis* [2006]. We used a spline interpolation function to build the Brunt-Väisälä profile $N(z)$ from the potential density anomaly derived from the CTD legs of the AUV G2 Slocum glider. We plot in Figure A1 a characteristic density profile obtained outside of (a) the mesoscale anticyclone, (b) the corresponding Brunt-Väisälä frequency, and (c) the vertical profile of the first baroclinic eigenmode.

The first baroclinic deformation radius corresponding to this summer stratification is $R_{d,1} = 13$km (this Rossby radius is noted R_d in the present study). This value is smaller than the climatological value in the area, according to *Chelton et al.* [1998]. The node of the first baroclinic eigenmode fixes the thickness of the upper and the lower layer for an equivalent two-layer system. According to Figure 6, the characteristic thickness of the upper layer is $h = 120$ m. This value is significantly deeper than the extreme of N located $50 - 60$ m below the sea surface.
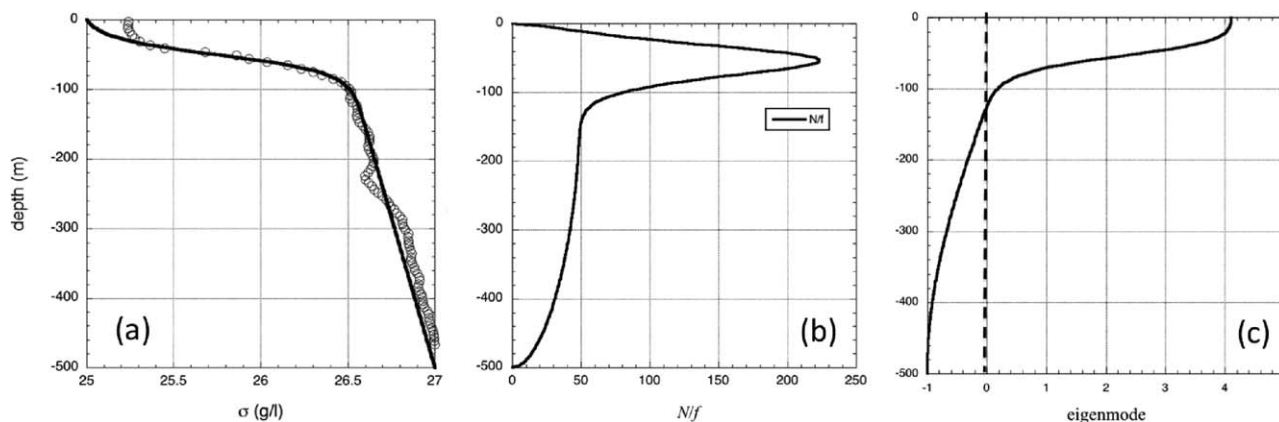

Figure A1. (a) Vertical profile of the potential density anomaly $\sigma(z)$ sampled outside the vortex, (b) the corresponding Brunt-Väisälä frequency in dimensionless units $N(z)/f$ and (c) the vertical structure of the first baroclinic eigenmode computed using equation (A1).

References

Adduce, C., and C. Cenedese (2004), An experimental study of a mesoscale vortex colliding with topography of varying geometry in a rotating fluid, *J. Mar. Res.*, *62*(5), 611–638.

Andres, M., and C. Cenedese (2013), Laboratory experiments and observations of cyclonic and anticyclonic eddies impinging on an island, *J. Geophys. Res. Oceans*, *118*, 762–773, doi:10.1002/jgrc.20081.

Arístegui, J., P. Sangrà, S. Hernández-León, M. Cantón, A. Hernández-Guerra, and J. L. Kerling (1994), Island-induced eddies in the Canary islands, *Deep Sea Res., Part I*, *41*(10), 1509–1525.

Barton, E. D., G. Basterretxea, P. Flament, E. G. Mitchelson-Jacob, B. Jones, J. Arístegui, and F. Herrera (2000), Lee region of Gran Canaria, *J. Geophys. Res.*, *105*(C7), 17,173–17,193, doi:10.1029/2000JC900010.

Bibby, T. S., M. Y. Gorbunov, K. W. Wyman, and P. G. Falkowski (2008), Photosynthetic community responses to upwelling in mesoscale eddies in the subtropical North Atlantic and Pacific Oceans, *Deep Sea Res., Part II*, *55*(10–13), 1310–1320.

Caldeira, R. M. A., and P. Marchesiello (2002), Ocean response to wind sheltering in the Southern California Bight, *Geophys. Res. Lett.*, *29*(13), 1635, doi:10.1029/2001GL014563.

Caldeira, R. M. A., and P. Sangrà (2012), Complex geophysical wake flows, *Ocean Dyn.*, *62*(5), 683–700.

Caldeira, R. M. A., and R. Tomé (2013), Wake response to an ocean-feedback mechanism: Madeira Island case study, *Boundary Layer Meteorol.*, *148*, 419–436.

Caldeira, R. M. A., S. Groom, P. Miller, D. Pilgrim, and N. P. Nezlin (2002), Sea-surface signatures of the island mass effect phenomena around Madeira Island, Northeast Atlantic, *Remote Sens. Environ.*, *80*(2), 336–360.

Calil, P. H. R., K. J. Richards, Y. Jia, and R. R. Bidigare (2008), Eddy activity in the lee of the Hawaiian Islands, *Deep Sea Res., Part II*, *55*(10–13), 1179–1194.

Carnevale, G. F., R. C. Kloosterziel, P. Orlandi, and D. J. van Sommeren (2011), Predicting the aftermath of vortex breakup in rotating flow, *J. Fluid Mech.*, *669*, 90–119.

Cenedese, C. (2002), Laboratory experiments on mesoscale vortices colliding with a seamount, *J. Geophys. Res.*, *107*(C6), 3053, doi:10.1029/2000JC000599.

Cenedese, C., C. Adduce, and D. M. Fratantoni (2005), Laboratory experiments on mesoscale vortices interacting with two islands, *J. Geophys. Res.*, *110*, C09023, doi:10.1029/2004JC002734.

Chang, M.-H., T.-Y. Tang, C.-R. Ho, and S.-Y. Chao (2013), Kuroshio-induced wake in the lee of Green Island off Taiwan, *J. Geophys. Res.*, *118*, 1508–1519, doi:10.1002/jgrc.20151.

Chavanne, C., P. Flament, and K.-W. Gurgel (2010), Interactions between a Submesoscale Anticyclonic Vortex and a Front, *J. Phys. Oceanogr.*, *40*(8), 1802–1818.

Chelton, D. B., R. A. deSzoeke, M. G. Schlax, K. El Naggar, and N. Siwertz (1998), Geographical Variability of the First Baroclinic Rossby Radius of Deformation, *J. Phys. Oceanogr.*, *28*(3), 433–460.

Coutis, P. F., and J. H. Middleton (2002), The physical and biological impact of a small island wake in the deep ocean, *Deep Sea Res., Part I*, *49*(8), 1341–1361.

Couvelard, X., R. M. A. Caldeira, I. B. Araujo, and R. Tome (2012), Wind mediated vorticity-generation and eddy-confinement, leeward of the Madeira Island: 2008 numerical case study, *Dyn. Atmos. Oceans*, *58*, 128–149.

Dietrich, D. E., M. J. Bowman, C. A. Lin, and A. Mestas-Nunez (1996), Numerical studies of small island wakes in the ocean, *Geophys. Astrophys. Fluid Dyn.*, *83*(3–4), 195–231.

Dong, C., and J. C. McWilliams (2007), A numerical study of island wakes in the Southern California Bight, *Cont. Shelf Res.*, *27*(9), 1233–1248.

Dong, C., J. C. McWilliams, and A. F. Shchepetkin (2007), Island wakes in deep water, *J. Phys. Oceanogr.*, *37*(4), 962–981.

Dugan, J. P., R. P. Mied, P. C. Mignerey, and A. F. Schuetz (1982), Compact, intrathermocline eddies in the Sargasso Sea, *J. Geophys. Res.*, *87*(C1), 385–393.

Feldman, C. G., and C. R. McClain (2007), Ocean color web processing flags and masks, SeaWiFS reprocessing 5.1 and MODIS-aqua reprocessing 1.1, technical report.

Feldman, G. C., and C. R. McClain (2012), Ocean Color Web, MODIS Reprocessing R2009, NASA Goddard Space Flight Center, edited by N. Kuring, S. W. Bailey. [Available at http://oceancolor.gsfcnasa.gov/.]

Godfrey, J. S. (1989), A sverdrup model of the depth-integrated flow for the world ocean allowing for island circulations, *Geophys. Astrophys. Fluid Dyn.*, *45*(1–2), 89–112.

Gordon, A., C. F. Giulivi, C. M. Lee, H. H. Furey, A. Bower, and L. Talley (2002), Japan/East Sea intrathermocline eddies, *J. Phys. Oceanogr.*, *32*(6), 1960–1974.

Hasegawa, D., H. Yamazaki, R. G. Lueck, and L. Seuront (2004), How islands stir and fertilize the upper ocean, *Geophys. Res. Lett.*, *31*, L16303, doi:10.1029/2004GL020143.

Hasegawa, D., M. R. Lewis, and A. Gangopadhyay (2009), How islands cause phytoplankton to bloom in their wakes, *Geophys. Res. Lett.*, *36*, L20605, doi:10.1029/2009GL039743.

Heywood, K. J., D. P. Stevens, and G. R. Bigg (1996), Eddy formation behind the tropical island of Aldabra, *Deep Sea Res., I*, *43*(4), 555–578, doi:10.1016/0967-0637(96)00097-0.

Hogan, P. J., and H. E. Hurlburt (2006), Why do intrathermocline eddies form in the Japan/East Sea? A modeling perspective, *Oceanogr. Lit. Rev.*, *19*(3), 134–143.

Jackson, C. P. (2006), A finite-element study of the onset of vortex shedding in flow past variously shaped bodies, *J. Fluid Mech.*, *182*, 23–45.

Jia, Y., P. H. R. Calil, E. P. Chassignet, E. J. Metzger, J. T. Potemra, K. J. Richards, and A. J. Wallcraft (2011), Generation of mesoscale eddies in the lee of the Hawaiian Islands, *J. Geophys. Res.*, *116*, C11009, doi:10.1029/2011JC00730.

Jiménez, B., P. Sangrà, and E. Mason (2008), A numerical study of the relative importance of wind and topographic forcing on oceanic eddy shedding by tall, deep water islands, *Ocean Modell.*, *22*(3–4), 146–157.

Kersalé, M., A. M. Doglioli, and A. A. Petrenko (2011), Sensitivity study of the generation of mesoscale eddies in a numerical model of Hawaii islands, *Ocean Sci.*, *7*(3), 277–291.

Kloosterziel, R. C., and G. J. F. van Heijst (2006), An experimental study of unstable barotropic vortices in a rotating fluid, *J. Fluid Mech.*, *223*, 1–24.

Kostianoy, A. G., and I. M. Belkin (1989), A survey of observations on emtrathermocline eddies in the world ocean, in *Elsevier Oceanography Series*, vol. 50, edited by J. C. J. Nihoul and B. M. Jamart, 821–841, doi:10.1016/S0422-9894(08)70223-X.

Kunze, E. (1985), Near-inertial wave propagation in geostrophic shear, *J. Phys. Oceanogr.*, *15*(5), 544–565.

Kunze, E. (1986), The mean and near-inertial velocity fields in a warm-core ring, *J. Phys. Oceanogr.*, *16*(8), 1444–1461.

Ladd, C. (2005), Observations from a Yakutat eddy in the northern Gulf of Alaska, *J. Geophys. Res.*, *110*, C03003, doi:10.1029/2004JC002710.

Ladd, C., W. R. Crawford, C. E. Harpold, W. K. Johnson, N. B. Kachel, P. J. Stabeno, and F. Whitney (2009), A synoptic survey of young meso-scale eddies in the Eastern Gulf of Alaska, *Deep Sea Res. Part II*, *56*(24), 2460–2473.

Lazar, A., A. Stegner, and E. Heifetz (2013a), Inertial Instability of Intense Stratified Anticyclones. Part I: Generalised stability criterion, *J. Fluid Mech.*, *732*, 457–484.

Lazar, A., Stegner, A., R. Caldeira, C. Dong, H. Didelle, and S. Vibound (2013b), Inertial instability of intense stratified anticyclones: Part 1: Generalized stability criterion, *J. Fluid Mech.*, *732*, 485–509.

Mackas, D. L., and M. D. Galbraith (2002), Zooplankton distribution and dynamics in a North Pacific eddy of coastal origin: I. Transport and loss of continental margin species, *J. Oceanogr.*, *58*(5), 725–738.

Marshall, J., and F. Schott (1999), Open-ocean convection: Observations, theory, and models, *Rev. Geophys.*, *37*(1), 1–64.

Martins, C. S., M. Hamann, and A. F. G. Fiuza (2002), Surface circulation in the eastern North Atlantic, from drifters and altimetry, *J. Geophys. Res.*, *107*(C12), 3217, doi:10.1029/2000JC000345.

McGillicuddy, D. J., et al. (2007), Eddy/wind interactions stimulate extraordinary mid-ocean plankton blooms, *Science*, *316*(5827), 1021–1026.

Morel, Y., and J. McWilliams (1997), Evolution of isolated Interior Vortices in the Ocean, *J. Phys. Oceanogr.*, *27*, 727–748.

Morel, Y., and L. N. Thomas (2009), Ekman drift and vortical structures, *Ocean Modell.*, *27*(3–4), 185–197.

Nauw, J. J., H. M. van Aken, J. R. E. Lutjeharms, and W. P. M. de Ruijter (2006), Intrathermocline eddies in the Southern Indian Ocean, *J. Geophys. Res.*, *111*, C03006, doi:10.1029/2005JC002917.

Patzert, W. C. (1969), Eddies in Hawaiian waters, HIG Rep. HIG-69-8, 51 pp., Hawaii Institute of Geophysics, University of Hawaii at Manoa, Honolulu, Hawaii.

Pedlosky, J., L. J. Pratt, M. A. Spall, and K. Helfrich (1997), Circulation around islands and ridges, *J. Mar. Res.*, *55*, 1199–1251.

Perret, G., A. Stegner, M. Farge, and T. Pichon (2006a), Cyclone-anticyclone asymmetry of large-scale wakes in the laboratory, *Phys. Fluids*, *18*(3), 036,603-036,603-11.

Perret, G., A. Stegner, T. Dubos, J. M. Chomaz, and M. Farge (2006b), Stability of parallel wake flows in quasigeostrophic and frontal regimes, *Phys. Fluids*, *18*(12), 126602, doi:10.1063/1.2397563.

Piedeleu, M., P. Sangrà, A. Sánchez-Vidal, J. Fabrés, C. Gordo, and A. Calafat (2009), An observational study of oceanic eddy generation mechanisms by tall deep-water islands (Gran Canaria), *Geophys. Res. Lett.*, *36*, L14605, doi:10.1029/2008GL037010.

Poulain, P.-M., and E. Zambianchi (2007), Surface circulation in the central Mediterranean Sea as deduced from Lagrangian drifters in the 1990s, *Cont. Shelf Res.*, *27*(7), 981–1001.

Sangrà, P. (2005), Life history of an anticyclonic eddy, *J. Geophys. Res.*, *110*, C03021, doi:10.1029/2004JC002526.

Sangrà, P., M. Auladell, A. Marrero-Díaz, J. L. Pelegrí, E. Fraile-Nuez, A. Rodríguez-Santana, J. M. Martín, E. Mason, and A. Hernández-Guerra (2007), On the nature of oceanic eddies shed by the Island of Gran Canaria, *Deep Sea Res., Part I*, *54*(5), 687–709.

Sangrà, P., et al. (2009), The Canary Eddy Corridor: A major pathway for long-lived eddies in the subtropical North Atlantic, *Deep Sea Res., Part I*, *56*(12), 2100–2114.

Siedler, G., A. Kuhl, and W. Zenk (1987), The Madeira Mode Water, *J. Phys. Oceanogr.*, *17*, 1561–1570.

Snyder, C., D. J. Muraki, R. Plougonven, and F. Zhang (2007), Inertia–gravity waves generated within a dipole vortex, *J. Atmos. Sci.*, *64*(12), 4417–4431.

Stegner, A. (2014), Oceanic island wake flow in laboratory, in *Modelling Atmospheric and Oceanic Flows Insights From Laboratory Experiments and Numerical Simulations, Geophys. Monogr. Ser.,* vol. 205, edited by T. von Larcher and P. D. Williams, AGU, Washington, D. C. and Wiley, Hoboken, N. J.

Stegner, A., T. Pichon, and M. Beunier (2005), Elliptical-inertial instability of rotating Karman vortex streets, *Phys. Fluids*, *17*(6), 066,602, doi:10.1063/1.1937348.

Teinturier, S., A. Stegner, H. Didelle, and S. Viboud (2010), Small-scale instabilities of an island wake flow in a rotating shallow-water layer, *Dyn. Atmos. Oceans*, *49*(1), 1–24.

Tomczak, M. (1988), Island wakes in deep and shallow water, *J. Geophys. Res.*, *93*(C5), 5153–5154.

Vallis, G. K. (2006), *Atmospheric and Oceanic Fluid Dynamics: Fundamentals and Large-scale Circulation*, 745 pp., Cambridge Univ. Press, Cambridge, U.K.

Wen, C. Y., and C. Y. Lin (2001), Two-dimensional vortex shedding of a circular cylinder, *Phys. Fluids*, *13*(3), 557–560.

Yoshida, S., B. Qiu, and P. Hacker (2010), Wind-generated eddy characteristics in the lee of the island of Hawaii, *J. Geophys. Res.*, *115*, C03019, doi:10.1029/2009JC005417.